A NOVEL MOLECULAR SIMULATION APPROACH TO LIQUID-LIQUID EQUILIBRIA AND APPLICATION TO THE DESIGN OF DESALINATION SOLVENTS

By

PRASHANTH CHANDRAN

Bachelor of Technology in Chemical Engineering
Anna University
Chennai, India
2016

Submitted to the Faculty of the
Graduate College of
Oklahoma State University
in partial fulfillment of
the requirements for
the Degree of
Master of Science
May 2018

A NOVEL MOLECULAR SIMULATION APPROACH TO LIQUID-LIQUID EQUILIBRIA AND APPLICATION TO THE DESIGN OF DESALINATION SOLVENTS

Thesis Approved:

Jindal K. Shah

Thesis Advisor

Sundar V. Madihally

Craig R. Bradshaw

ACKNOWLEDGMENTS

First of all, I would like to thank my advisor Dr. Jindal Shah for giving me an opportunity to work in this interesting thesis topic. His teachings, suggestions and guidance was instrumental for me in completing this thesis. His thermodynamics course has helped me in developing ideas many of which forms the crux of this work. I have always enjoyed the meetings with him where we discuss in-depth about various ideas and concepts. He has been a great mentor from the day I got to work with him and has always been an inspiration to me. Having learned a lot from him both professionally as well as personally, I would like to wholeheartedly thank him. I would also like to thank my thesis committee members Dr. Sundar Madihally and Dr. Craig Bradshaw for giving me useful inputs on my thesis which has helped me to learn more and bring about the completion of my thesis into a good shape. Special mention to Dr. Bradshaw's course on Advanced Thermal Systems which I have thoroughly enjoyed and it helped in clarifying my questions which had puzzled me during my undergraduate years. I would like to Acknowledge the National Science Foundation for funding this project and the OSU High Performance Computing Center at Oklahoma State University for giving me access to the computing nodes on which I ran all of the simulations required for this thesis. My family has been very supportive to me in pursuing my career and also when I moved to the United States from India to start my Master's degree. Finally, I would also like to give special regards to my friends in Stillwater who have made this place a home away from home for me.

Acknowledgments reflect the views of the author and are not endorsed by committee members or Oklahoma State University.

Name: Prashanth Chandran

Date of Degree: May 2018

Title of Study: A NOVEL MOLECULAR SIMULATION APPROACH TO LIQUID-LIQUID EQUILIBRIA AND APPLICATION TO THE DESIGN OF DESALINATION SOLVENTS

Major Field: CHEMICAL ENGINEERING

Abstract: Conventionally, seawater desalination involves energy-intensive distillation or pressure-driven membrane processes. Recent studies show that directional solvent extraction (DSE) could serve as a viable low-temperature and low-energy alternative. This method utilizes a solvent capable of selectively dissolving water by rejecting the salt ions and at the same time having negligible solubility in water phase followed by the extraction of the dissolved water by heating or cooling the solvent phase. Octanoic acid and decanoic acid have been discovered to serve as a viable candidate for DSE solvent with all the desirable properties. Their studies have shown that these solvents have very low effectiveness of extracting water and thus need better solvent with good water extracting capacity for making the process more efficient. Such a solvent can be identified by screening molecules capable of extracting higher amount of water than octanoic acid and decanoic acid using a computational approach. Success of such a screening process critically depends on the ability to calculate the solubility of water in solvents and requires *a priori* prediction of liquid-liquid equilibria of the solvent and water. These calculations remain challenging from molecular simulations due to the difficulties associated with the transfer of molecules between two dense liquid phases. In order to overcome these limitations, a novel molecular simulation methodology is developed based on computing the fugacity of water as a function of concentration to calculate the water dissolution in a range of solvents assuming that the solubility of the solvent is negligible in water. The calculated solubilities are shown to yield good agreement with experimental data for long chain carboxylic acids over a range of temperatures. After developing the method, different solvents were studied which includes branched and fluorinated structures of octanoic acid. Also, the effect of adding alcohol functional group to the molecule at different positions was also studied. Finally, the developed method was also extended to study systems showing mutual solubility in both the directions and was demonstrated using butanol-water system.

TABLE OF CONTENTS

LIST OF TABLES

Table Page

LIST OF FIGURES

NOMENCLATURE

f ..... Fugacity
P ..... Pressure
T ..... Temperature
v ..... Molar Volume
x ..... Mole fraction

Subscripts/Superscripts

$'$ ..... Phase 1
$''$ ..... Phase 2
0 ..... Pure component
1 ..... Component 1 or water
2 ..... Component 2 or solvent
∞ ..... Infinite dilution
mix ..... Mixture
res ..... Residual

Greek Symbols

μ ..... Chemical potential
γ ..... Activity coefficient

CHAPTER 1

Introduction

1.1 Water Scarcity

Access to fresh water is the most basic necessity for any life on the earth. However, many factors such as population growth, industrialization, climate change, etc., have led to water scarcity in many regions around the world. The World Economic Forum's Global Risks Report 2017 listed water scarcity to be one of the leading crises. [2] Figure 1.1 gives the map showing the extent of water stress in the world countries and a analysis has showed that 37 countries are currently facing extremely high levels of water stressed conditions. [1] Regions such as the Middle East, California, Texas, Arizona, Central Asia are known to be facing physical water scarcity caused by the unavailability of fresh water. Another condition of water scarcity known as the economic water scarcity denotes the condition wherein water is present however the lack of infrastructure, poor water management owing to under-development and poverty causes the demand for water. This is prevalent in developing regions such as the South Asia, Sub-Saharan Africa and Central America. Another study has shown that about 4 billion people in the world are facing water scarcity atleast one month a year. [3]

1.2 Water Desalination

Only 2.5% of the world's water resource is freshwater and of this about 68.7% is contained in glaciers and icecaps, 30.1% in the form of underground water with only 1.2% being available from surface fresh water sources [4]. Though the problem of water

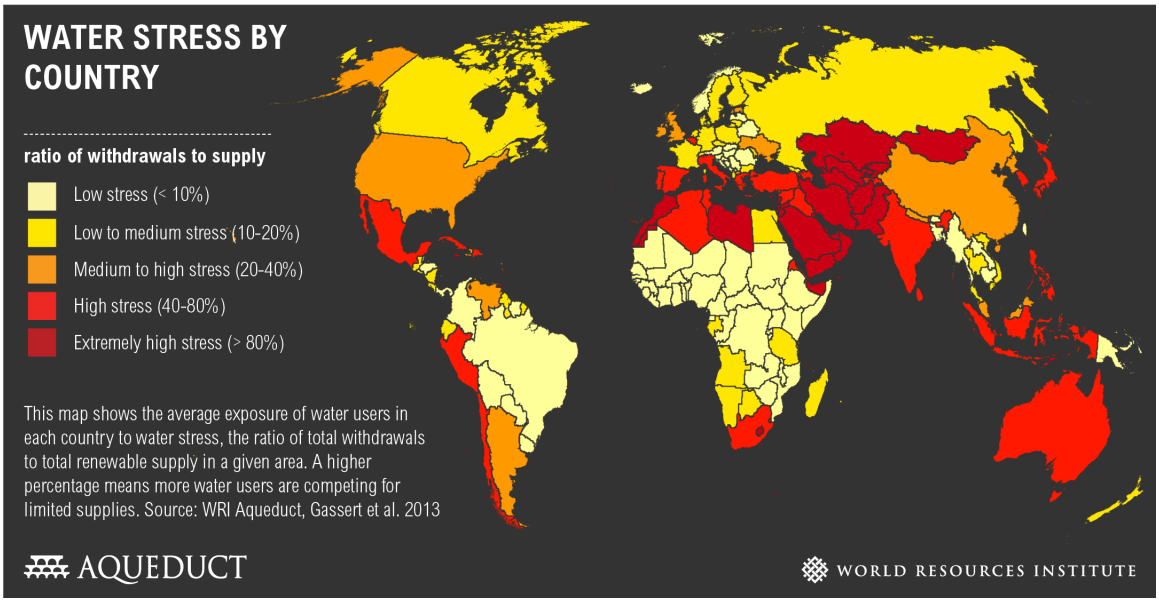

Figure 1.1: Map showing the extent of water stress for the world countries [1]

scarcity can be approached by adopting better water management schemes, water recycle, conservations, etc., desalination of sea water is the only alternative available beyond the natural fresh water resources to increase the water supply [5]. This is supported by the fact that oceans constitiues about 96.5% of the world water [4] and seawater could prove to be an inexhaustible source for meeting the water demand, provided the availability of effective techniques for desalination [6]

1.3 Sea Water Desalination technologies

By the end of 2015, the total production capacity of desalination in the world was 22,870 million gallons per day produced from about 18000 desalination plants [7]. All of the major desalination techniques can either be classified as membrane process or thermal process with the former accounting for about 63.7% of the global production and the latter of about 34.2% [8]. Membrane process includes methods such as reverse osmosis, forward osmosis, nanofiltration and electrodialysis. All these method employs membranes of one form or the other. Thermal process includes multistage flash distillation, multi-effect distillation, vapor compression distillation and

humidification-dehumidification process. In-spite of these technologies, desalination accounts for about just 1% of the global water supply [7]. The reason for this could be attributed to the high cost involved in the operation and maintenance of these plants. Membrane process are usually pressure driven which requires the use of higher grade of energy in the form of electricity. In addition, these membranes requires frequent maintenance and replacement due to factors such as fouling and damage caused by the saline water and high pressure. Thermal process though using a lower grade of energy in the form of heat, it involves evaporation of water to separate it from the salts and hence would require high amount of energy supplied as latent heat.

1.4 Directional Solvent Extraction

Recently, a novel method of desalination known as Directional Solvent Extraction was demonstrated [9]. It involves the use of no membranes and can operate at temperatures as low as 40°C to 70°C. The process employs a solvent which can selectively extract water by rejecting the salt ions [10, 11]. It was shown that the process could work under moderate conditions of pressure and temperature unlike the other current desalination techniques this process can operate satisfactorily with waste heat which is abundantly available from many sources. The method is devoid of disadvantages such as fouling and high pressure operations that are prevalent in membrane techniques and the latent heat required as in thermal processes.

Figure 1.2 gives the process flow diagram of a continuous directional solvent extractions process for saline water desalination. Initially, the saline water and the directional solvent are mixed together and then heated to a higher temperature. The solvent is not completely miscible with the saline phase and hence it phase separates when allowed to settle. At the same time, the solvent selectively dissolves some amount of water into it by rejecting the salt ions or having very negligible solubility of

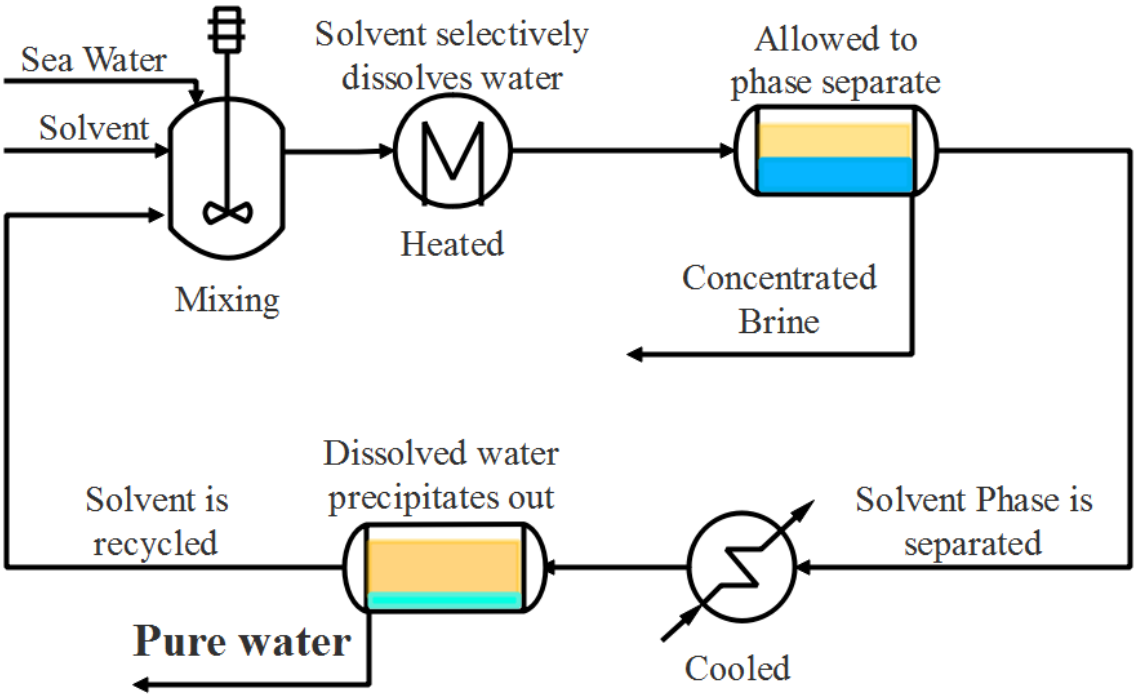

Figure 1.2: Process flow Diagram illustrating a continuous Directional Solvent Extraction (DSE) desalination

the salts. However, the solvent would possess very negligible solubility into the aqueous phase and hence the name directional solvent extraction. After phase separation, the organic/solvent phase and the aqueous phase are separated. The aqueous phase would have a higher salinity and hence can be rejected as brine or recycled back to the saline water feed. The solvent phase which is saturated with water is cooled down to a lower temperature owing to which some amount of water separates into a different phase due to the reduction in solubility at this reduced temperature. Now this water phase can be drawn out as desalinated water after allowing sufficient time for phase separation. The solvent phase can now be recycled. Based on this process, it can be inferred that the following are the ideal characteristics for a directional solvent:

- Immiscible with water
- Dissolves water into its phase
- Has appreciable Temperature dependent solubility of water

- Negligibly soluble into the water phase
- Rejects salt ions

Octanoic acid and decanoic acid are such directional solvents which were shown to have these desired characteristics [9]. The carboxylic acid functional group is polar and can form hydrogen bonds with water molecules and hence has the capability to dissolve water. At the same time, the long non-polar alkyl part keeps it immiscible with water and reduces its solubility into the aqueous phase. They were also shown to have good ion rejection properties [9, 11]. However, these solvents suffers from low effectiveness. For example, decanoic acid has an effectiveness of about 1% for a temperature pair of 34°C and 55°C. Effectiveness can be defined as the kilograms of desalinated water recovered for every 100 kilograms for solvent circulated through the process. This low effectiveness needs the use of huge amount of solvent circulation and the associated energy consumption required for heating, cooling and pumping tends to be higher. Thus the discovery of solvents with better water yielding capacity can improve the overall cost or energy efficiency of DSE process [12, 13].

1.5 Molecular Simulation of Liquid-Liquid Equilibria

In order to find solvents for DSE with better effectiveness than octanoic acid and decanoic acid, a large number of solvents would needed to be studied and screened. This would require a thorough knowledge on the liquid-liquid equilibria (LLE) between the solvent, water and the salt ions. Experimental determination of liquid-liquid equilibria could prove to be tedious as it is required to do these studies for a large number of solvents as a function of temperature. In addition, the cost incurred for setting up the experiments and acquiring all the solvents might also be a lot. These days, molecular simulations are being widely used for phase equilibria studies and for high throughput screening of large number of molecules as a substitute for experimental studies. These can be described as computational experiments wherein molecular models are used to

predict the properties of compounds and they offer a lot of flexibility. For instance, a solvent which has never been discovered or synthesized can also be simulated and studied. Thus, it can be used as a tool for the initial computational screening of solvents that can be used in the DSE process by studying the LLE between the solvent and water with out the need for experimental studies.

Molecular simulation study of liquid-liquid equilibria is usually performed using the method of Gibbs ensemble Monte Carlo (GEMC) which was proposed and originally illustrated for vapor-liquid equilibrium and simple osmotic systems by Panagiotopoulos [14, 15]. To date, it remains the most widely applied method and has been extended to simple Lennard-Jones systems and complex molecular mixtures [16, 17, 18, 19, 20, 21, 22, 23, 24, 25, 26, 27, 28]. Chemical equilibirum is acheived between the two phases by the transfer of molecules between the phases in addition to the translational and volume change moves to realize thermal and pressure equilibria. In the case of liquid-liquid equilibria, these molecular transfer moves tend to have a very poor acceptance rate owing to the two dense liquid phases in the simulation and the insertion moves are usually accompanied by overlap with the neighboring molecules.

To overcome these sampling challenges associated with the transfer of particles between two dense liquid phases, several techniques have been proposed and employed along with GEMC such as the configurational-bias Monte Carlo [29, 30, 31, 32, 33], continuous fractional component Monte Carlo [34, 35], utilizing a third ideal vapor box setup [36, 26, 28], etc. Attempts have also been made to predict LLE using molecular dynamics simulation such as isomolar semigrand ensemble molecular dynamics [37], computing chemical potentials [10, 38], temperature quench molecular dynamics [39] and direct coexistence method [40]. In spite of these advances, determi-

nation of LLE continues to be challenging in the field of molecular simulations owing to the associated challenges such as aggregation, poor acceptance rates for particle transfer and the small transfer free energy of solvation in certain systems. [28]

In order to overcome these challenges, an entirely different approach has been adopted in this work that was inspired from the works of Paluch et al. [41, 42] wherein the solubility of several pharmaceutically relevant compounds was computed in pure and binary solvents. In the process of which the authors derived an expression for the infinite dilution fugacity expressed in terms of the molar volume of the solvent and the residual chemical potentials of water. In this work, using this relation, fugacity was computed by adopting molecular dynamics simulations to compute the molar volume and residual chemical potential with the later being determined by the method of thermodynamic integration [43]. Unlike the GEMC method, thermodynamic integration does not involves the less efficient molecular transfer moves. Instead it computes the free energy difference by gradual insertion of a molecule by turning on or tuning off its interaction step wise which gives the residual chemical potential. Hence the fugacity of water in the solvent rich phase was computed as a function of mole fraction of water. By equating this to the fugacity of pure water, the equilibrium composition of water in the solvent-rich phase was obtained. This approach is based on the assumption that the water-rich phase has a very dilute concentration of solvent. This is a reasonable assumption for long chain organic compounds such as directional solvents investigated in this work owing to the relatively long non-polar hydrophobic alkyl chain in the molecule which keeps its concentration low in the water-rich phase. Once the concentration of the solvent-rich phase is known, the fugacity of the pure solvent is computed, which in turn is equated to the fugacity of solvent in water at infinite dilution to ascertain the dilute level concentration of fatty acid in the water-rich phase. Details of this method can be found in chapter 2.

Using this method, a few possible candidates as a directional solvent was designed by studying their properties. Taking octanoic acid as a base structure, the effect of branching, fluorination, addition of hydroxyl functional group and position of the functional group on the effectiveness of the solvent and the solvent loss in pure aqueous phase were studied. This methodology can also be applied for any systems in which the concentration of one of the components is dilute in another phase which can come across is any engineering or scientific study. In addition, the method was extended to binary systems showing appreciable mutual solubility in both the phases. This is done by rewriting the fugacity equation to give the activity coefficients. Now, using molecular simulations, this quantity can be found for both the components. An activity model is fitted to this data and is used for determining the equilibrium compositions of the two phases at the particular temperature.

1.6 Outline of Thesis

This thesis is organized as follows. In chapter 2, the theory behind the development of the method used to study directional solvents is given. Also, it contains the theory used for extending the same method and developing a generalized molecular simulation LLE prediction method is presented. Chapter 3 gives the details on the forcefield/molecular models used for modeling the molecules used in this study is explained followed by the details of performing and setting up the simulations.

In chapter 4, first the developed method is demonstrated and validated for the directional solvents previously studied namely hexanoic acid, octanoic acid and decanoic acid. The obtained compositions of the solvent and water rich phase were compared with experimental data available from literature. In addition, the molecular level structural properties which gives rise to the observed macroscopic behavior is pre-

sented. Then the developed method is used to study different candidates for DSE by having the octanoic acid as the base structure. Effectiveness, defined as the kilograms of water that can be recovered for every cubic meter of solvent between the temperatures of 20°C and 50°C, was used to compare solvents. Finally, the extended method applicable for mutually soluble systems is applied to the binary butanol-water system and its phase equilibria was generated and compared with the experimental data.

CHAPTER 2

Theory

2.1 Directional Solubility

For a binary liquid-liquid system, the equilibrium conditions at a constant temperature T and pressure P are given by the equality of the fugacity of each components in both the phases (eqs. 2.1 and 2.2):

$$f_1(x_1', T, P) = f_1(x_1'', T, P) \tag{2.1}$$

$$f_2(x_2', T, P) = f_2(x_2'', T, P) \tag{2.2}$$

where f_1 and f_2 refer to the the fugacity of water (component 1) and solvent (component 2), respectively. x_1 and x_2 denote the mole fractions of water and solvent with the single and the double primes symbolizing the water rich and solvent rich phases, respectively.

2.1.1 Solubility of water in solvent rich phase

The fugacity of water in the water rich phase (The left hand side of equation 2.1) can be written in terms of the activity coefficient and pure liquid fugacity:

$$f_1(x_1', T, P) = x_1' \gamma_1(x_1', T, P) f_1^0 \tag{2.3}$$

where γ_1 is the activity coefficient of water and f_1^0 is the liquid phase fugacity of pure water. As previously stated, it is expected that the solubility of the solvent in the

water rich phase is negligible, implying $x_1' \approx 1$ and $\gamma_1(x_1', T, P) \approx 1$. Thus, equation 2.3 reduces to:

$$f_1(x_1', T, P) = f_1^0 \tag{2.4}$$

Using eqs. 2.4 and 2.1 leads to:

$$f_1(x_1'', T, P) = f_1^0 \tag{2.5}$$

From the above equation, it is clear that if the fugacity of water is known as a function of concentration, the water solubility in the solvent rich phase is that corresponding to the concentration that yields pure water fugacity. Following Noroozi and Paluch [42], the fugacity of a species, such as water in this case, can be expressed in terms of its residual chemical potential, molar volume of the mixture and the species mole fraction as:

$$\ln f_1(x_1'', T, P) = \frac{\mu_1^{\text{res}}(x_1'', T, P)}{RT} - \ln \frac{v_{\text{mix}}(x_1'', T, P)}{RT} + \ln x_1'' \tag{2.6}$$

where μ_1^{res} is the residual chemical potential of water, v_{mix} is the molar volume of the mixture and R is the universal gas constant. Equation 2.6 provides a route to calculating the fugacity, which involves the determination of residual chemical potential and the mixture molar volume at a mole fraction of x_1''; the residual chemical potential can be obtained using any free energy method while the mixture molar volume is available from an isothermal-isobaric ensemble molecular dynamics simulation. In an analogous manner, the liquid phase fugacity of pure water is obtained by setting the mole fraction to unity:

$$\ln f_1^0 = \frac{\mu_1^{\text{res},0}(T, P)}{RT} - \ln \frac{v_1(T, P)}{RT} \tag{2.7}$$

where $\mu_1^{\text{res},0}(T,P)$ is the residual chemical potential of pure water and v_1 is the corresponding molar volume. Equations 2.6 and 2.7 are substituted in eq. 2.5 to solve for the equilibrium composition of the solvent rich phase.

2.1.2 Solubility of solvent in the water rich phase

To obtain the solubility of the solvent in the water rich phase, equation 2.6 is written, in terms of the fugacity of the solvent, for both the phases as:

$$\ln f_2(x_2', T, P) = \frac{\mu_2^{res}(x_2', T, P)}{RT} - \ln \frac{v_{mix}(x_2', T, P)}{RT} + \ln x_2' \tag{2.8}$$

$$\ln f_2(x_2'', T, P) = \frac{\mu_2^{res}(x_2'', T, P)}{RT} - \ln \frac{v_{mix}(x_2'', T, P)}{RT} + \ln x_2'' \tag{2.9}$$

where μ_2^{res} refers to the residual chemical potential of solvent at a given concentration. Under the condition that the concentration of solvent is dilute in the water phase, the residual chemical potential and the molar volume are approximated to the infinite dilute residual chemical potential $\mu_2^{\text{res},\infty}(T,P)$, and pure water molar volume, $v_1(T,P)$, respectively. Thus, equation 2.8 reduces to:

$$\ln f_2(x_2', T, P) = \frac{\mu_2^{res,\infty}(T, P)}{RT} - \ln \frac{v_1(T, P)}{RT} + \ln x_2' \tag{2.10}$$

Equating eqs. 2.9 and 2.10 and rearranging for the concentration of solvent in the water rich phase yields:

$$x_2' = \frac{x_2'' v_1(T,P)}{v_{\text{mix}}(x_2'', T, P)} \exp\left(\frac{\mu_2^{res}(x_2'', T, P) - \mu_2^{res,\infty}(T, P)}{RT}\right) \tag{2.11}$$

Once the solubility of the water, x_1'', in the solvent rich phase is known, using the fact that for a binary mixture $x_2'' = 1 - x_1''$, the values of $\mu_2^{res}(x_2'', T, P)$ and $v_{\text{mix}}(x_2'', T, P)$ are obtained by molecular simulations as detailed below. The residual chemical potentials are then used in eq. 2.12 to estimate the concentration of the solvent in the

water rich phase.

Equation 2.12 was used for the results of water rich phase given in figure 4.3. For the remain calculations and comparative study starting from section 4.1.4, equation 2.12 was modified as follows by assuming the solvent rich phase to be pure.

$$x_2' = \frac{v_1(T,P)}{v_2(T,P)} \exp\left(\frac{\mu_2^{res,0}(T,P) - \mu_2^{res,\infty}(T,P)}{RT}\right) \tag{2.12}$$

Here, v_2 gives the molar volume of pure solvent, $\mu_2^{res,0}(T,P)$ is the residual chemical potential of pure solvent. This assumption was made to get an initial estimate of the solvent loss as this equation does not require the knowledge of the composition of the solvent rich phase prior hand and hence the simulations can be run simultaneously without having to wait for the results of the solvent rich phase.

2.2 Mutual Solubility

To extend this method to the systems showing appreciable mutual solubility in both the directions found widely in chemical engineering applications, the method developed was extended to predict the mutual solubility of such systems. In this case, the assumption that one of the component is sparingly soluble in the other phase is not valid. Equation 2.3 can be rewritten to give the activity coefficient of the first component as a function of composition:

$$\gamma_1(x_1,T,P) = \frac{f_1(x_1,T,P)}{x_1 f_1^0} \tag{2.13}$$

This can be rewritten as:

$$\ln \gamma_1(x_1,T,P) = \ln f_1(x_1,T,P) - \ln x_1 - \ln f_1^0 \tag{2.14}$$

Now, using equation 2.6 and 2.7 in equation 2.14 gives:

$$\ln \gamma_1(x_1, T, P) = \frac{\mu_1^{\text{res}}(x_1, T, P) - \mu_1^{\text{res},0}(T, P)}{RT} + \ln \frac{v_1(T, P)}{v_{\text{mix}}(x_1, T, P)} \tag{2.15}$$

Similarly, the activity coefficient of the second component can be written as:

$$\ln \gamma_2(x_2, T, P) = \frac{\mu_2^{\text{res}}(x_2, T, P) - \mu_2^{\text{res},0}(T, P)}{RT} + \ln \frac{v_2(T, P)}{v_{\text{mix}}(x_2, T, P)} \tag{2.16}$$

Using equation 2.15 and 2.16, the activity coefficients of both the components can be found as a function of composition using the residual chemical potentials and molar volumes obtained from molecular dynamics simulations. Once they are known, they can be fitted to a suitable activity coefficient model. In this work, NRTL model was used to fit the activity coefficient data. Now, the equilibrium composition of both the phases can be obtained by solving for the iso-activity equations derived from equation 2.1 and 2.2:

$$x_1' \gamma_1(x_1', T, P) = x_1'' \gamma_1(x_1'', T, P) \tag{2.17}$$

$$x_2' \gamma_2(x_2'', T, P) = x_2'' \gamma_2(x_2'', T, P) \tag{2.18}$$

Thus x_1' and x_1'' can be determined using the expressions $x_2' = 1 - x_1'$ and $x_2'' = 1 - x_1''$.

CHAPTER 3

Simulation Methodology and Details

3.1 Force Field/Molecular Models

Force fields can be defined as the molecular models which describes the energetics of intermolecular and intramolecular interactions arising in molecular systems. These interactions are the ones which give rise to the observable macroscopic properties. In this work, OPLS-AA force field [44] was used for modeling the solvent molecules while water was represented by the TIP4P model. [45] The non-bonded interactions, comprised of the Lennard-Jones 12-6 potential and the Coulombic interactions, were calculated using the functional form:

$$E_{\text{non-bonded}} = \sum_{i<j} 4\epsilon_{ij} \left[\left(\frac{\sigma_{ij}}{r_{ij}} \right)^{12} - \left(\frac{\sigma_{ij}}{r_{ij}} \right)^{6} \right] + \sum_{i<j} \frac{q_i q_j}{4\pi\epsilon_o r_{ij}} \tag{3.1}$$

where σ_{ij}, ϵ_{ij} are the Lennard-Jones diameter and well depth, repsectively for the pair of atoms i and j, q_i and q_j are the respective partial charges and r_{ij} represents the separation between the sites. Geometric combining rule was used for both the Lennard-Jones parameters of unlike interactions. All the non-bonded interactions, in a molecule, between the pair of atoms separated by less than 3 bonds were excluded while the interactions were scaled by a factor of 0.5 for those pairs connected through exactly three bonds. The bond lengths were constrained at their equilibrium values by parallel linear constraint solver.[46] The bonded interactions included those arising from bond angle bending and torsion which were calculated using the following

functional forms:

$$E_{\text{angles}} = \sum_{\text{angles}} K_\theta \left(\theta - \theta_o\right)^2 \tag{3.2}$$

$$E_{\text{dihedrals}} = \sum_{\text{dihedrals}} \left[\sum_{i=1}^{4} K_i \left(1 + (-1)^{i+1} \cos(i\phi)\right)\right] \tag{3.3}$$

Here, K_θ and K_i refers to the force constants for the bonds and dihedrals. θ refers to the bond angle and θ_0 denotes the equilibrium bond angle. ϕ refers to the dihedral angle.

3.2 Simulation Methodology

Simulations were carried out using the molecular dynamics package GROMACS-5.0.4. [47] The solvent rich phase was simulated with 200 solvent molecules while the number of water molecules was set according to the mole fraction being simulated. 600 water molecules were used to compute properties for the pure water phase. The initial configurations were generated with PACKMOL [48] followed by a steepest descent energy minimization in GROMACS. The system was then equilibrated in the canonical ensemble (NVT) for 200 ps using Berendsen thermostat and isothermal-isobaric (NPT) ensemble for 1 ns. The temperature and pressure in the NPT simulation were controlled with a Berendsen thermostat and barostat. Additional 1 ns of NPT equilibration was then performed using the Nosé-Hoover thermostat and Parrinello-Rahman barostat. Finally, the production run was performed with the same thermostat and barostat for 5 ns. Time constants of 0.2 ps and 0.4 ps were used for the Berendsen and Nosé-Hoover thermostats, respectively. For both the Berendsen and Parrinello-Rahman barostats, the time constant was set to 2 ps. Pure and mixture molar volumes for use in equations 2.6 – 2.12 were obtained from these production runs. In all the cases, the pressure was maintained at 1 bar. The Lennard-Jones interactions were truncated at a distance of 12 Å by gradually switching off the interactions starting from 8 Å. Long-range electrostatic interactions were

computed with Particle-mesh Ewald method.[49]

For hexanoic acid and octanoic acid, the simulations were conducted at the temperatures of 293.15, 303.15, 313.15 and 323.15 K, whereas for decanoic acid, temperatures of 308.15, 313.15, 318.15 and 323.15 K were employed. The temperatures were selected considering the available literature experimental data for comparison.

For the calculation of residual chemical potentials, thermodynamic integration [43] was employed. In this method, a solute molecule interacts with the system through a coupling parameter λ that controls the strength of interaction between the solute molecule and the system. Simulations are carried out such that the coupling parameter spans a value from 0 to 1 representing the ideal gas state and the fully coupled state, respectively. The free energy change is then computed by

$$\Delta G = \int_0^1 \left\langle \frac{\partial H(\lambda)}{\partial \lambda} \right\rangle d\lambda. \tag{3.4}$$

In this equation, $H(\lambda)$ refers to the enthalpy of the system at a given coupling parameter. Due to the presence of both the Lennard-Jones and electrostatic interactions, the thermodynamic integration was carried out in two steps: the Lennard-Jones interactions were first scaled using 7 λ values (0, 0.1, 0.2, 0.4, 0.6, 0.8, 1) followed by increasing the partial charges on the molecule using 8 λ points (0, 0.2, 0.4, 0.6, 0.7, 0.75, 0.8, 0.9, 1) resulting in a fully coupled molecule. The free energy was evaluated using the GROMACS bar function. Statistical uncertainties were estimated by conducting three independent simulation for each λ. The protocol for the preparation of the system, subsequent equilibration, and data collection was identical to that described earlier.

CHAPTER 4

Results

4.1 Directional Solvents

4.1.1 Molar Volumes and Residual Chemical Potentials of Water in Octanoic Acid-Water System

In order to compute the solubility of water in the solvent rich phase from eq. 2.6, the mixture molar volumes and residual chemical potential as a function of the water concentration are required. The behavior of these quantities is illustrated with the octanoic-water system.

The top panel of Fig. 4.1 shows the molar volume for the octanoic acid-water system as a function of composition of water and temperature. It is clearly seen that the molar volume decreases with the increase in water concentration and increases with temperature at a given composition. The behavior is almost linear with respect to the mole fraction of water and hence a linear fit is used to find the molar volume behavior and used in equation 2.6. Black circles, red squares, green diamonds and blue triangles refer to the temperatures 293.15 K, 303.15 K, 313.15 K and 323.15 K respectively with the black solid, red dotted, green dashed and blue dot-dashed lines representing the corresponding linear fits.

The bottom plot of Fig. 4.1 illustrates the residual chemical potential for water in the octanoic acid-water system as a function of mole fraction of water and temperature.

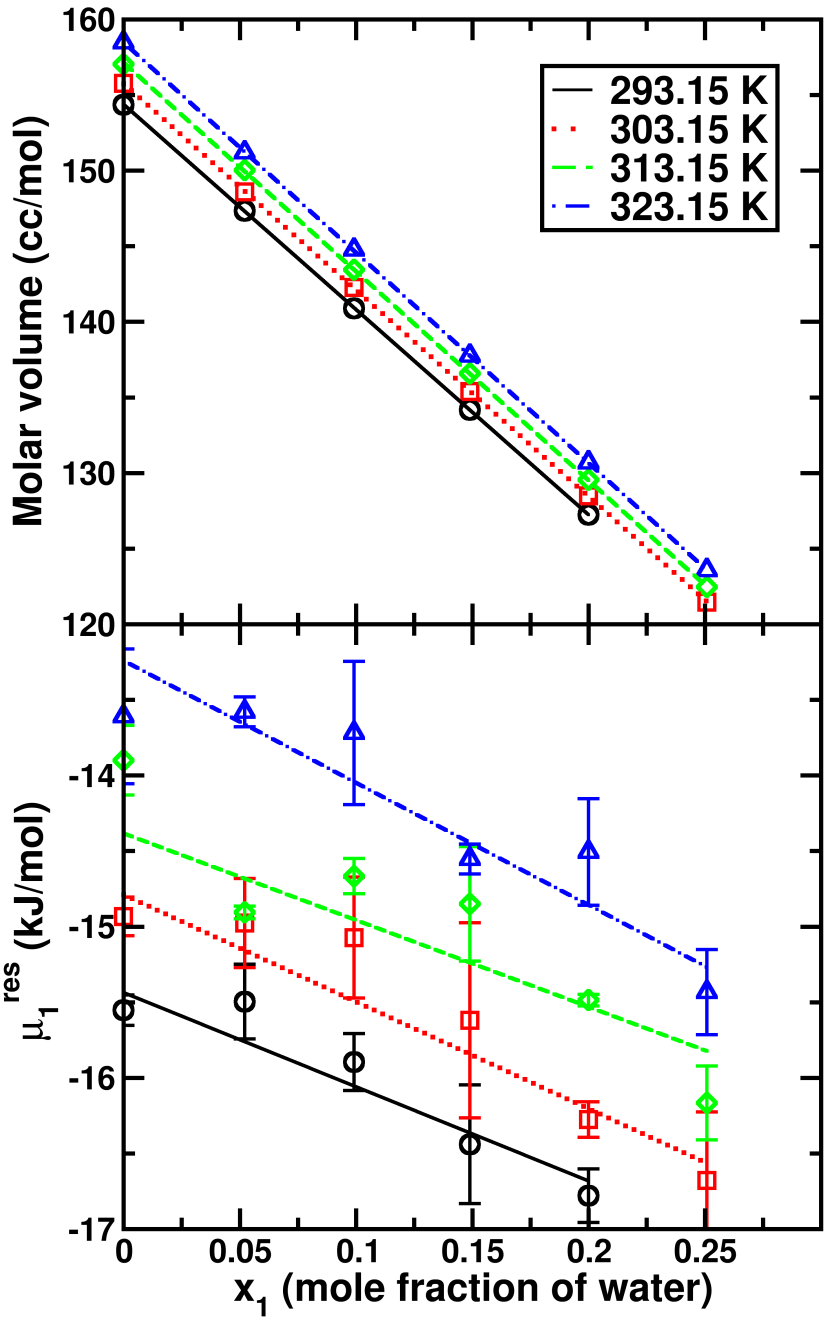

Figure 4.1: Molar volume and residual chemical potential of water as a function of composition for octanoic acid-water mixture

The behavior of residual chemical potential resembles that of the molar volume in that the residual chemical potential decreases (becomes more negative) with the increase in the water concentration, while it increases (less negative) with temperature. The data, at a given temperature, are represented by a linear fit to delineate the trend. In order to capture the non-linear behavior of the the residual chemical potential, a quadratic fit was also attempted. However, such a fit did not significantly affect the final calculated water solubility when compared to that obtained with a linear fit. Additionally, the errors associated with the coefficients in a quadratic fit tended to be high yielding higher uncertainty in the water solubility predictions. It should be emphasized that the percentage uncertainties in the residual chemical potential are larger than those obtained for the molar volumes, indicating well-known difficulties with calculating free energies. It can also be seen that, the uncertainties become more pronounced at higher water concentrations, probably due to the increasing aggregation of water as the two-phase region is approached.

The molar volume and the residual chemical potential at each of the water concentrations were substituted in equation 2.6 to obtain the fugacity values which are presented as symbols in Fig. 4.2. The fugacity curve, in Fig. 4.2, was obtained from the fits of the residual chemical potential and molar volume ensuring that these linear fits were truncated at the mole fraction for which the uncertainty in the fugacity value is within the pure water fugacity. It is seen that the resulting fugacity curve obtained from fits of the residual chemical potential and molar volume predicts the distinct fugacity values calculated at each of the mole fractions (represented by symbols) in very good agreement. Though it is possible to compute the fugacity in the two-phase region using this method, it is non-physical and hence these points are rejected. The equilibrium composition of the fatty acid rich phase is then obtained by the interpolation of the fugacity to match the pure water fugacity marked on the y-axis for

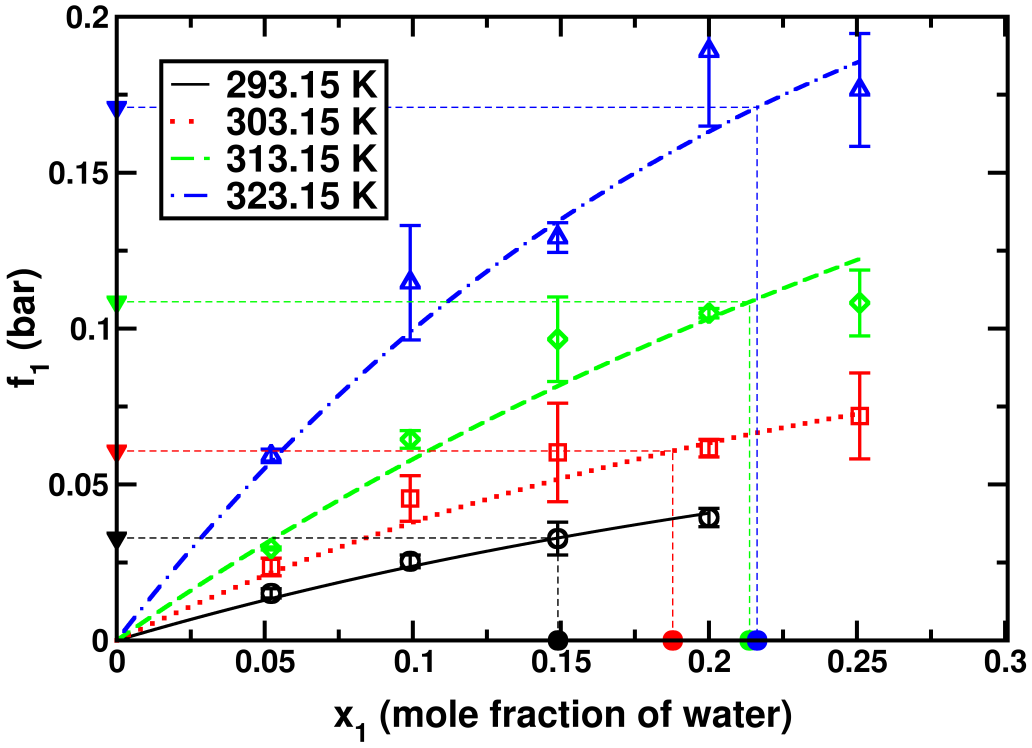

Figure 4.2: Fugacity of water vs. composition plot for octanoic acid-water mixture.

each of the temperatures. It is readily seen that the uncertainties associated with the residual chemical potential are reflected in the fugacity predictions, implying that any improvements in the calculations of residual chemical potentials would improve the statistical errors associated with the solubility predictions. This can be done by using more λ points for thermodynamic integration. However, this would increase the computational load. Nonetheless, with the current formulation, we were able to predict the residual chemical potential and the solubility with reasonable degree of error. Similar calculations were conducted for hexanoic acid and decanoic acid to compute the equilibrium concentration of water in the solvent rich phase at the respective temperatures. The data obtained from these systems are provided in the appendix. Open black circle, red square, green diamonds and blue triangles refer to the temperatures 293.15 K, 303.15 K, 313.15 K and 323.15 K, respectively with the

Temperature (K)	Fugacity of water (bar)			
	Pure phase	C6 rich phase	C8 rich phase	C10 rich phase
293.15	0.033 (00)	0.032 (07)	0.033 (06)	—
303.15	0.061 (00)	0.061 (04)	0.064 (08)	—
308.15	0.080 (00)	—	—	0.079 (11)
313.15	0.109 (01)	0.107 (05)	0.112 (19)	0.130 (19)
318.15	0.139 (02)	—	—	0.151 (16)
323.15	0.171 (00)	0.205 (07)	0.185 (15)	0.151 (11)

Table 4.1: Calculated fugacity of water in the pure phase and solvent rich phase. The figures in the parenthesis gives the standard error with respect to the last two decimal digits as calculated from three independent simulations

black solid, red dotted, green dashed and blue dot-dashed curves representing the corresponding functional form of fugacity obtained by using the linear fits of molar volumes and residual chemical potential in equation 2.6. The filled inverted triangles represent the fugacity of pure water and the filled circles denote the composition of the solvent rich phase at their respective temperatures corresponding to the colors. The thin dashed lines show the interpolation of equilibrium composition from pure water fugacity.

To confirm that the water concentrations obtained from fitting the fugacity represents true equilibrium, the fugacity of water at the estimated equilibrium concentration was calculated and the results are shown in Table 4.1. Overall the agreement is very good, indicating the proposed approach is capable of yielding equilibrium compositions in a liquid-liquid system.

Concentration of water in the solvent rich phase are displayed in Fig. 4.3 (top three plots) for the systems under consideration along with the experimental data. [50, 51]. It can be inferred that the solubility of water decreases with increase in the alkyl chain length in line with the experimental measurements. Moreover, increased solubilization of water with rise in temperature is predicted reasonably well by the force-field

employed in this work. The composition of the solvent rich phase for octanoic acid and decanoic acid are in very good agreement with the experimental data with average absolute deviation (AAD) of 0.016 and 0.021, respectively. However, relatively large AAD of 0.113 was observed for hexanoic acid. As hexanoic acid possesses relatively shorter alkyl chain, the assumption that hexanoic acid is infinitely dilute in the water rich phase under experimental conditions may have been violated; finite solubility of hexanoic acid in the water rich phase would change the fugacity of water that is in equilibrium with the water in the solvent rich phase.

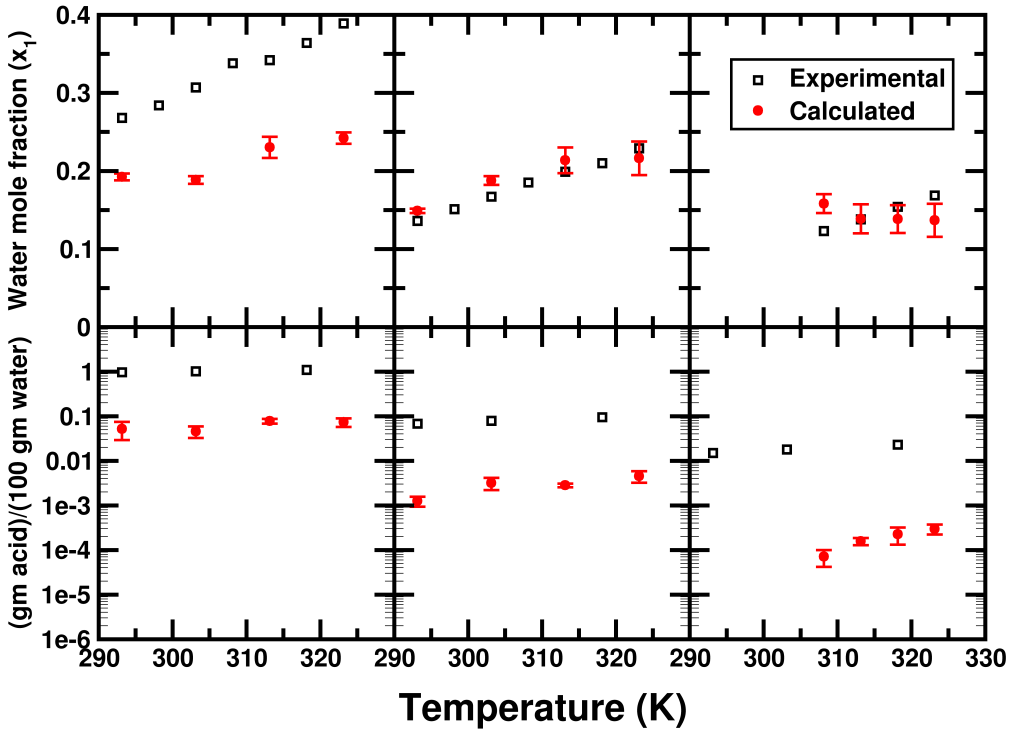

Figure 4.3: Composition of the solvent rich phase and water rich phase for hexanoic, octanoic and decanoic acid

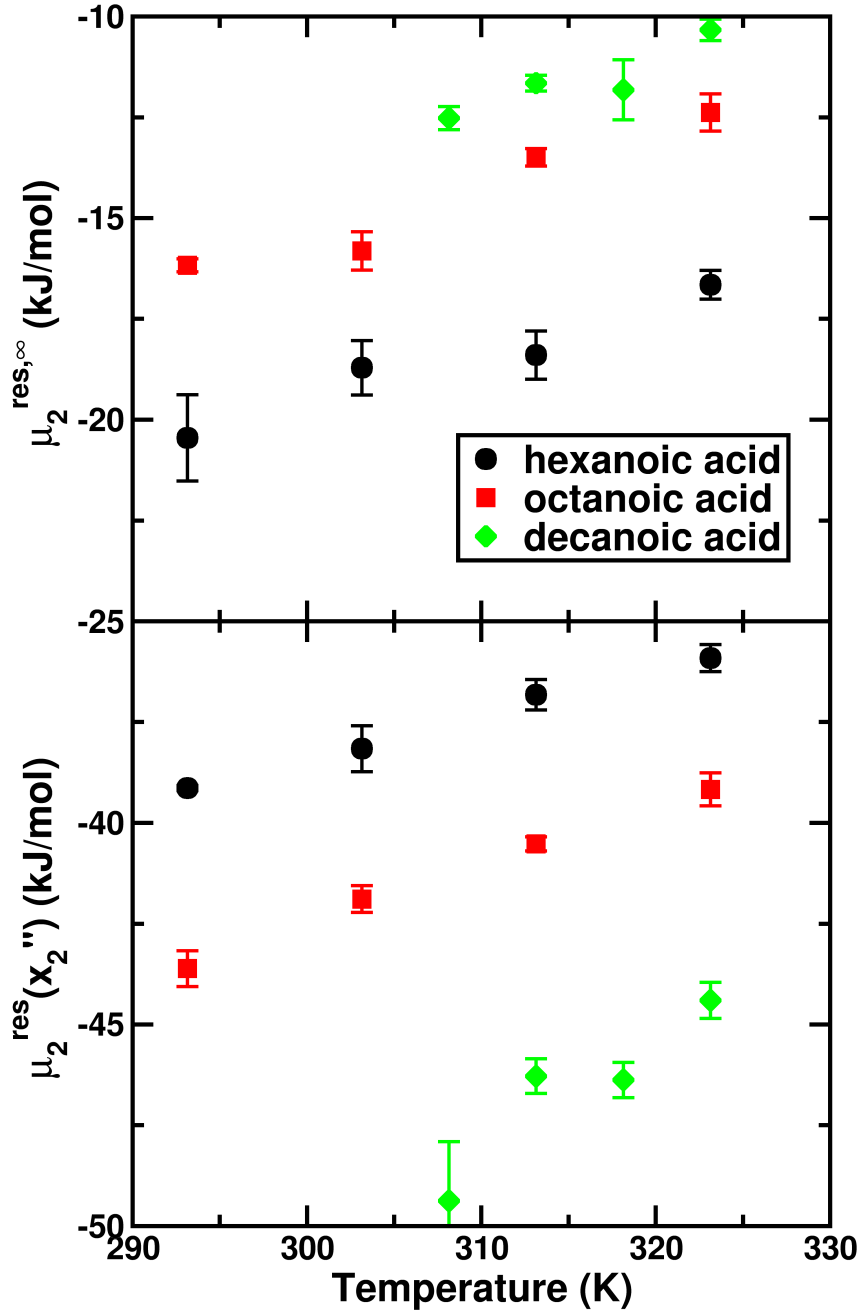

Figure 4.4: Residual chemical potential of solvent in the solvent rich phase (bottom) and infinite dilution residual chemical potential of solvent (top) as a function of temperature

4.1.2 Calculation of Solubility of Solvent in Water

Once the composition of the solvent rich phase is determined, the residual chemical potential of solvent in the organic rich phase is computed at the equilibrium compositions by finding the free energy change required for fully coupling a solvent molecule with the solvent-water system. The results of these calculations are shown in the bottom plot of Fig. 4.4. Two trends can be discerned from the data: (1) the residual chemical potential, for a given solvent, increases with increase in the temperature; (2) the residual chemical potential becomes more negative with longer alkyl chain. These trends can be explained based on the fact that the residual chemical potential refers to the free energy gained in transferring a gas phase molecule to the condensed phase. In the case of hexanoic acid, the free energy is the least negative at a given temperature primarily due to the high water concentrations in the system and relatively low stabilization of the molecule through van der Waals interactions as the alkyl chain is only six carbon long. On the other hand, the increase in the dispersion energy for the longer alkyl chain solvents coupled with low water concentrations results in higher favorable residual free energy for octanoic acid and decanoic acid. The infinite dilution free energy of transfer of solvents from gas phase to the water phase given by the top plot of Fig. 4.4 follows exactly the opposite trend due to the aforementioned reasons. These quantities when substituted in eq. 2.12 to calculate the composition of solvents in the water rich phase, which are displayed in the bottom pane of Fig. 4.3 along with the experimental results. As expected, the solvent concentrations in the water rich phase decrease with increase in the alkyl chain length, while an increase in the temperature leads to more dissolution of solvents in the water rich phase. The two observations are consistent with experimentally measured solubilities of solvents in the water rich phase.

However, it is to be noted that the solubility predictions of solvents in the water

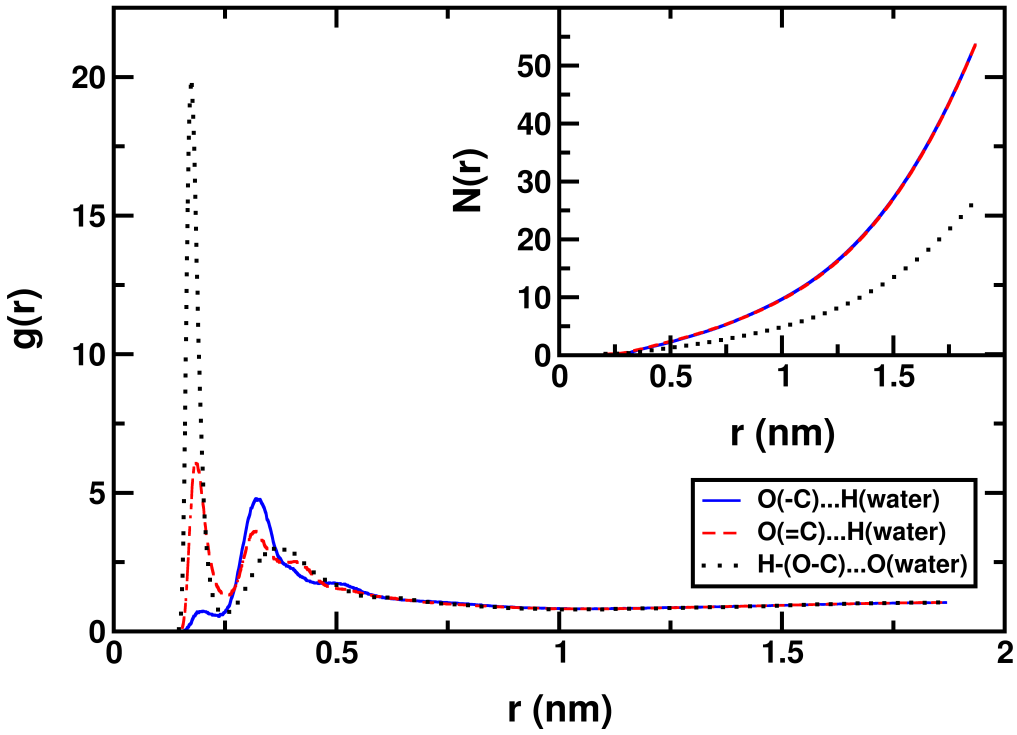

Figure 4.5: Radial distribution function for octanoic acid rich phase at 313.15 K

rich phase are consistently lower than the experimental results roughly by two orders of magnitude. The difference could be attributed to the extent to which water-solvent interactions are accurately captured by the force field models employed in this work. Another possibility is the neglect of the deprotonation of solvents in water. For example, the pKa values for hexanoic acid, octanoic acid, and decanoic acid are 4.88, 4.89 and 4.9 respectively, at 25°C [52]. Thus, it is conceivable that, in the experiments, the solubilities of deprotonated states were measured. Consequently, the negatively charged carboxylates would show higher solubilities in comparison to their undissociated neutral counterparts. The system size dependence on the solubilities was ruled out by computing the infinite dilute residual chemical potential of solvents in water by increasing the number of water molecules from 600 to 2100 in increments of 300; no statistical difference in the values for the residual chemical potential was observed.

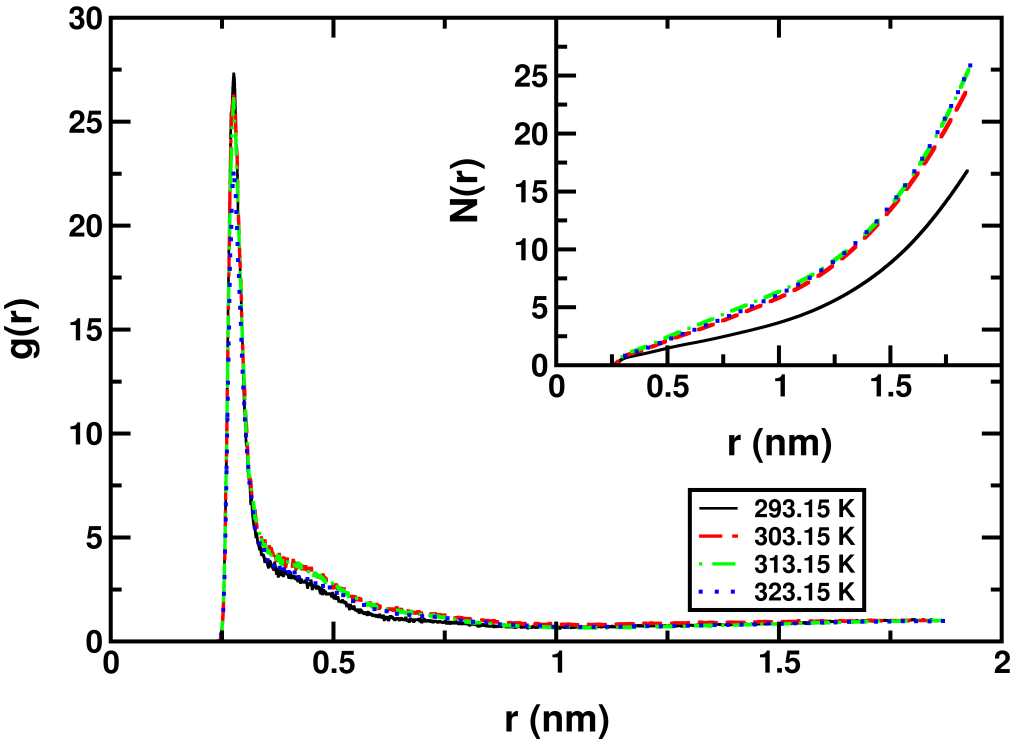

Figure 4.6: Oxygen-oxygen radial distribution function for water in octanoic acid rich phase

4.1.3 Structure of Solvent-Water Systems

It is instructive to examine the molecular level interaction between solvent and water to provide clues to the solubility of water in these systems. Fig. 4.5 displays the radial distribution functions (RDFs) in the octanoic acid rich phase at 313.15 K for three pairs of atoms based on potential for hydrogen bonding interactions: (a) carbonyl oxygen (solvent) - hydrogen (water); (b) hydroxyl oxygen (solvent) - hydrogen (water); (c) hydroxyl hydrogen (solvent) - oxygen (water). Black dotted, red dashed and blue solid curves represents the interactions for the pairs of hydroxyl hydrogen(solvent)-oxygen(water), carbonyl oxygen(solvent)-hydrogen(water) and hy-

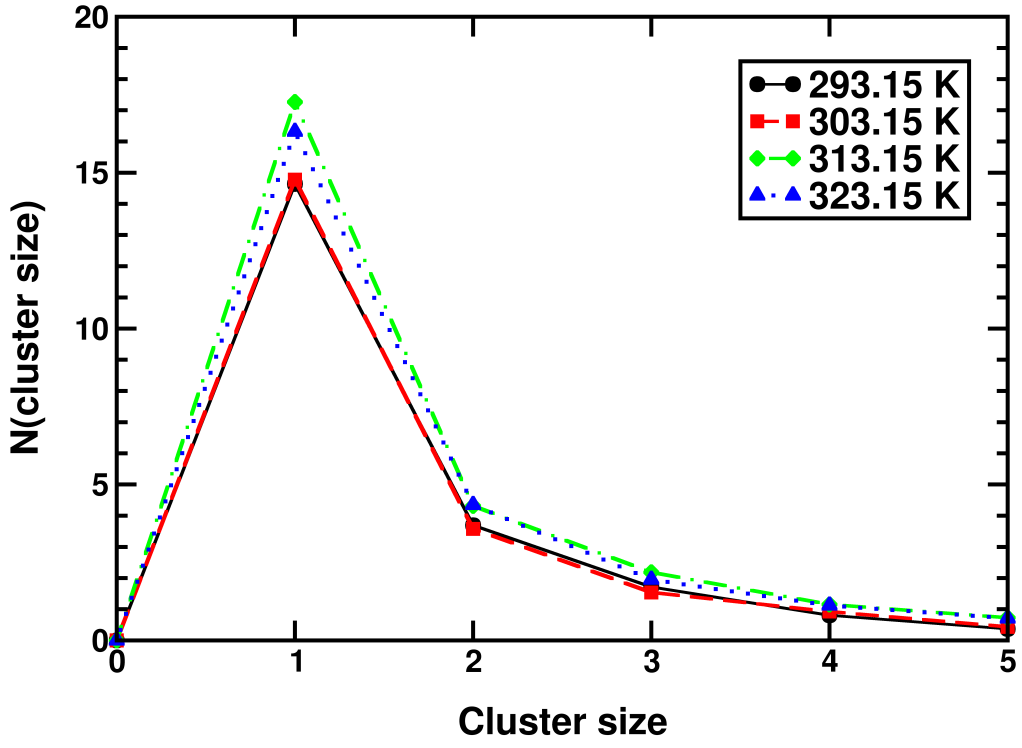

Figure 4.7: Cluster size distribution for water in octanoic acid rich phase

droxyl oxygen(solvent)-hydrogen(water) respectively. The inset gives the corresponding coordination numbers. All the RDFs are characterized by the first peak at ca. 0.2 nm, indicating that the three sites participate in the hydrogen bonding with water. Of these, the hydroxyl hydrogen shows the strongest peak indicating that it is the most preferred site for hydrogen bonding with water molecule followed by the carboxyl oxygen. Based on the first peak height, it can be inferred that the hydrogen bonding propensity of the water molecule for the hydroxyl oxygen is weaker in comparison to the other two sites. The second peak in the hydroxyl oxygen and carbonyl oxygen RDFs arises from the hydrogen atom of the same water molecule, which is not involved in the hydrogen bonding. In the case of hydroxyl hydrogen, however, the second peak represents the water molecule that is hydrogen bonded to the carbonyl oxygen.

Fig. 4.6 shows the oxygen-oxygen RDFs for the water molecules in the octanoic acid rich phase as a function of temperature. All the RDFs show the presence of a very strong first peak (>20), suggesting that water molecules are hydrogen bonded to other water molecules in the octanoic-water systems. The peak height, however, decreases with increase in the temperature, showing that the distribution of water molecules becomes more homogeneous (in comparison to that at the lowest temperature) around a given water molecule. This is analogous to the oxygen-oxygen RDF of ethanol in dodecane rich phase in the work by Harwood et al. [28] where the authors observed that increase in the concentration of ethanol in dodecane phase with temperature caused the decrease in peak height.

Further characterization of the structure of water aggregates in the octanoic acid-water system was probed by computing the cluster size distribution at each of the temperatures. For this analysis, two water molecules are assigned to the same cluster if the distance between their oxygen sites is within 0.35 nm, given by the first minimum in the oxygen-oxygen RDF. Fig. 4.7 presents the cluster size distribution for water molecules in the octanoic acid rich phase. At all the temperatures, monomers are the most prevalent with significant contributions from dimers and trimers. The dominance of monomers also suggests that the water molecules do not aggregate appreciably in the solvent rich phase. As an evidence of this conclusion, the average cluster size was calculated using eq. 4.1:

$$< S >= \frac{\sum_{i=1}^{n} i * N(i)}{\sum_{i=1}^{n} N(i)} \tag{4.1}$$

where i refers to the cluster size, $N(i)$ denotes the number of clusters found with a given cluster size and n gives the total number of water molecules. It was found

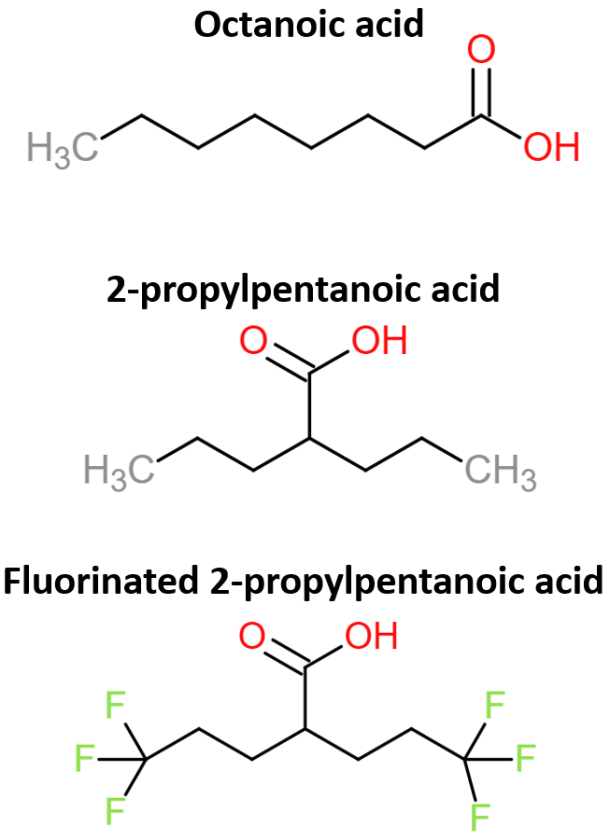

Figure 4.8: Structures used in branching and fluorination study

that the average cluster size of the water molecules is approximately 2 at all the temperatures, which is consistent with the fact that there are two different hydrogen bonding sites in octanoic acid.

4.1.4 Effect of Branching

Now having developed and demonstrated a method to study the water extraction capacity of directional solvents and their loss into the water phase, it is imperative to study other possible solvent candidates for DSE. So far, the molar volumes and residual chemical potential was determined as a function of mole fraction with an interval of 0.05. In the subsequent works shown from here, an interval of 0.1 was used. To begin with, in this study, octanoic acid was chosen as a base structure. Branched isomers of any linear organic molecules are generally known to be less hydrophobic than

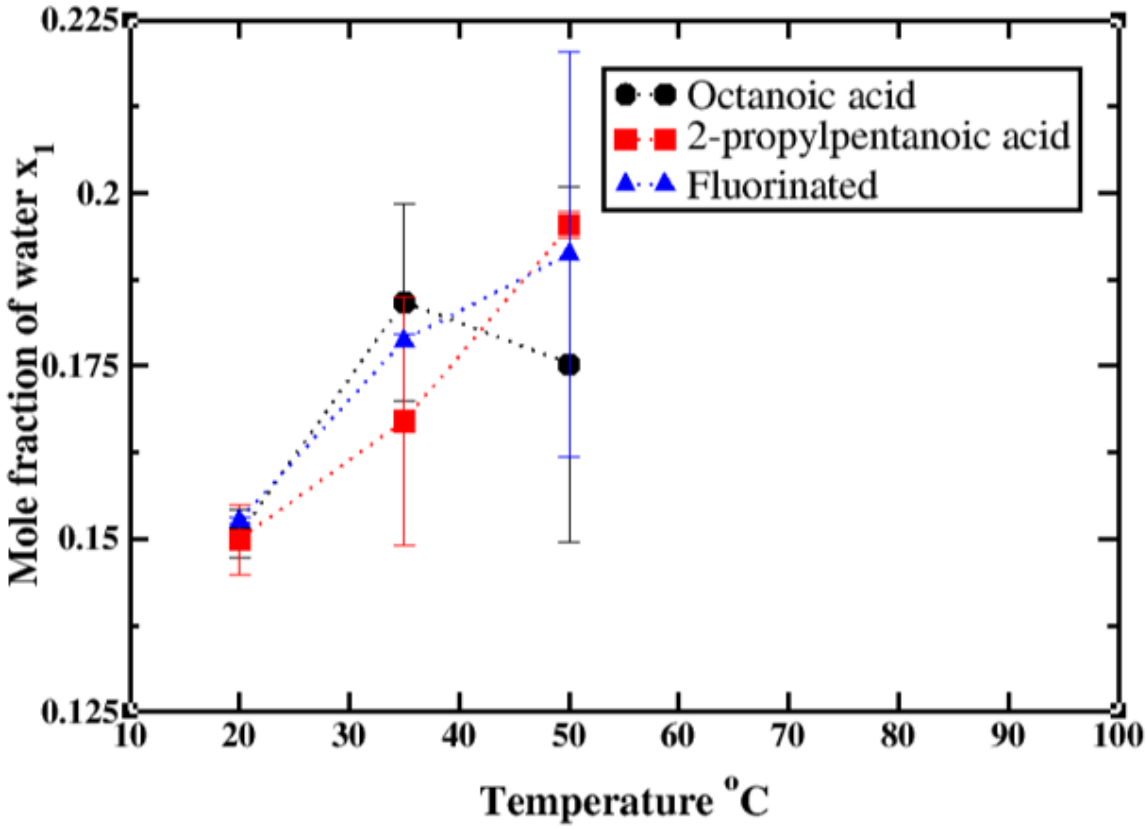

Figure 4.9: Solubility of water in solvent rich phase for branched and fluorinated structures

the original linear structures. Hence in this case, 2-propylpentanoic acid, a branched isomer of octanoic acid was studied and it was found that they have an effectiveness of 2.87 kg/m^3 and 5.34 kg/m^3, respectively. As expected, 2-propylpentanoic acid shows an increase in solubility of water at higher temperatures particularly at 50°C. The solubility of water can be seen from figure 4.9. This behavior can be explained as follows, branching in the alkyl chain decrease in hydrophobicity of the same because of the decrease in the overall surface area of the molecule. Also, the increased entropic contribution caused by the branched structure tends to accommodate more water molecules in the solvent rich phase. However, at the same time, this advantage of increased effectiveness of water extraction is accompanied by increase in the solvent loss into the water phase. Again, this is caused by the same phenomenon, wherein this branched structure needs lower free energy change for transferring it from the

solvent phase to water phase. This can be seen in figure 4.10 where it is evident that the solubility of the solvent in the water rich phase is higher for 2-propylpentanoic acid at all temperatures as opposed to octanoic acid.

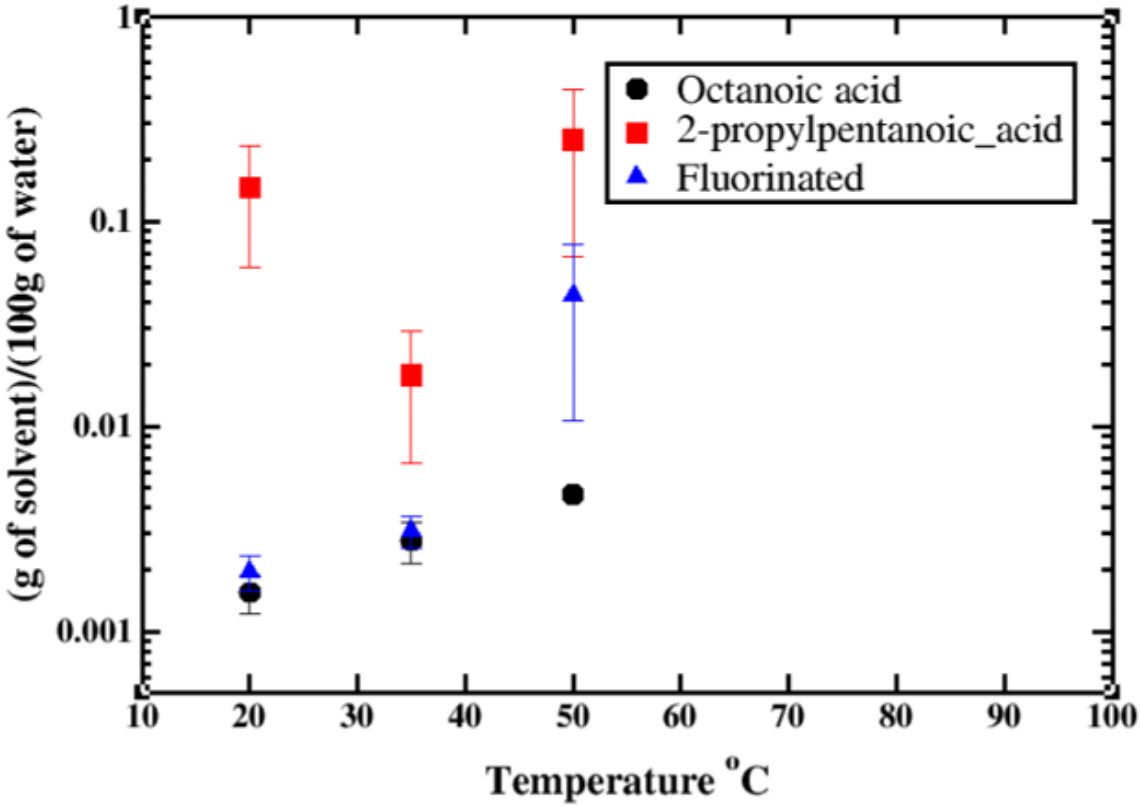

Figure 4.10: Solubility of solvent in water rich phase for branched and fluorinated structures

Since it is evident that branching increases the solubility in both the directions, taking 2-propylpentanoic acid, the structure was fluorinated at both the ends. That is, the -CH3 groups were replaced by -CF3 groups. This study was made because fluorinated alkyl groups are known to be more hydrophobic than normal hydrocarbons. Interestingly, fluorination of 2-propylpentanoic acid decreases the loss into the solvent phase making it on par with octanoic acid. At the same time, with an effectiveness of 3.81 kg/m^3, it has a better effectiveness than octanoic acid. These observations can be seen from figures 4.9 and 4.10. This is a significant result because, just by

fluorinating the alkyl chain of branched sturutes, we can see that the loss in solvent can be minimized with moderate reduction in extracting efficiency still remaining higher than the linear octanoic acid structure. Thus, fluorinated solvents can be proposed for experimental studies to see its feasibility for directional solvent extraction desalination. The molecular structures of octanoic acid, 2-propylpentanoic acid and fluorinated 2-propylpentanoic acid are shown in figure 4.8.

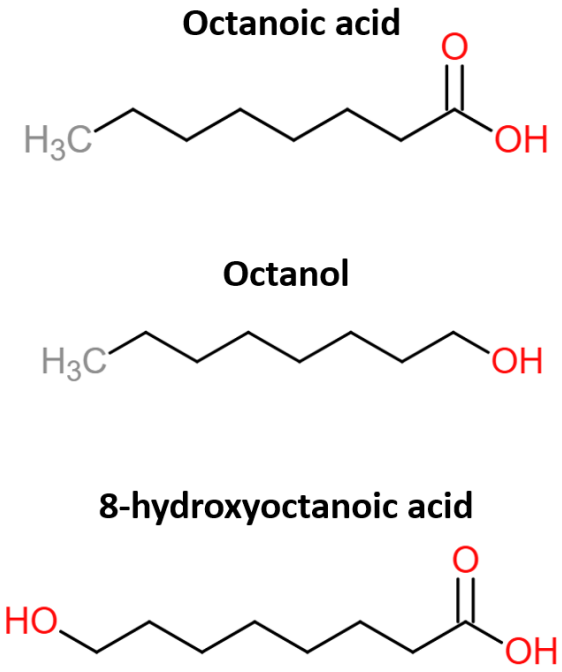

Figure 4.11: Structures used in alcohol functional group study

4.1.5 Addition of Alcohol Functional Group

As it was inferred from the radial distribution function of octanoic acid-water system in figure 4.5, the -OH group of the carboxylic acid functional group has got the highest affinity for water. Hence, a similar structure, to octanoic acid consisting of the alcohol functional group (-OH), octanol, was studied. In the case of the -COOH carboxylic functional group, there are two hydrogen bond recipients namely the hydroxyl oxygen and the carboxyl oxygen where the hydroxyl oxygen acts as a hydrogen bond donor

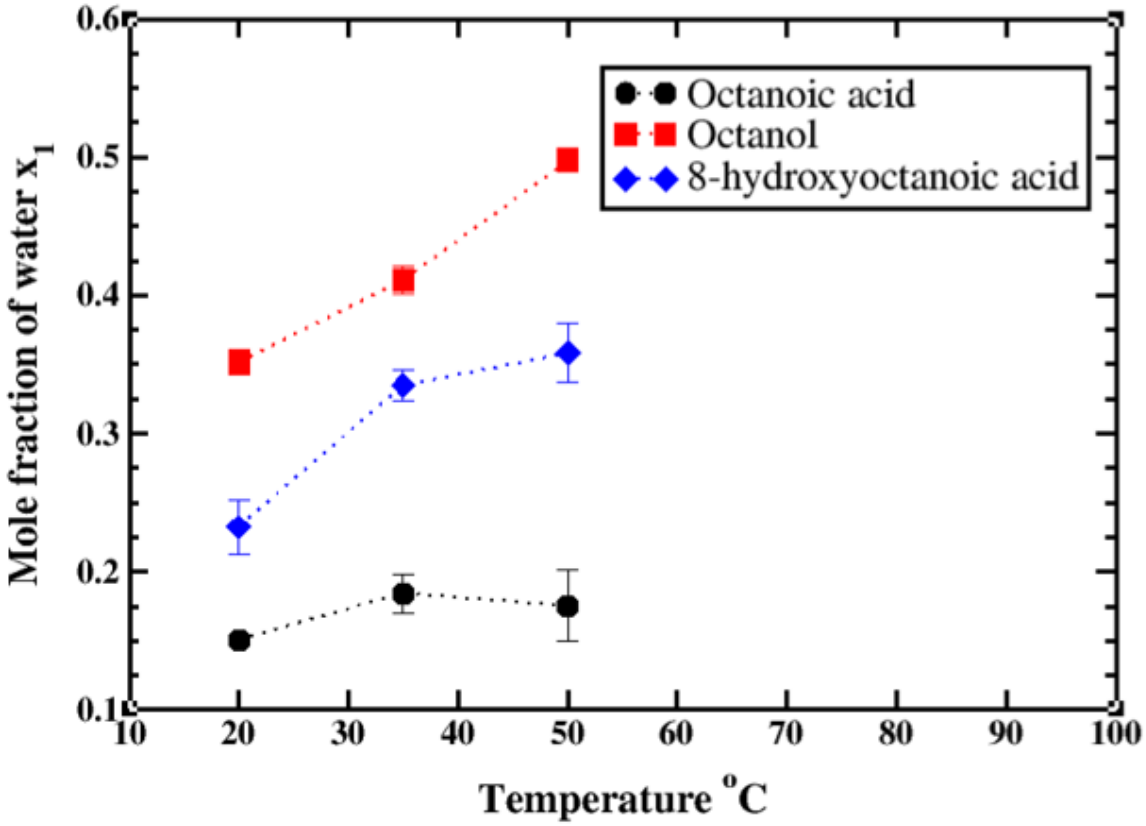

Figure 4.12: Solubility of water in solvent rich phase for branched and fluorinated structures

too. In the case of the -OH functional group, there is just one hydrogen bond donor as well as one recipient. Hence one might expect that octanol would be less hydrophilic than octanoic acid. However, octanol tends to have higher solubility of water, higher effectiveness of 16.89 kg/m^3 which is about six times that of octanoic acid as well as higher solvent loss in the water phase than octanoic acid at all temperatures. These can be seen from the concentration of the solvent rich and water rich phase given in figure 4.12 and 4.13. Though octanoic acid has got more hydrogen bonding sites than octanol, octanoic acid tends to associate within the surrounding octanoic acid molecules leaving fewer sites for dissoluting water. In addition, this also increases the transfer free energy into the water phase for octanoic acid when compared to octanol. Thus we are encountering the above described phase equilibria with water.

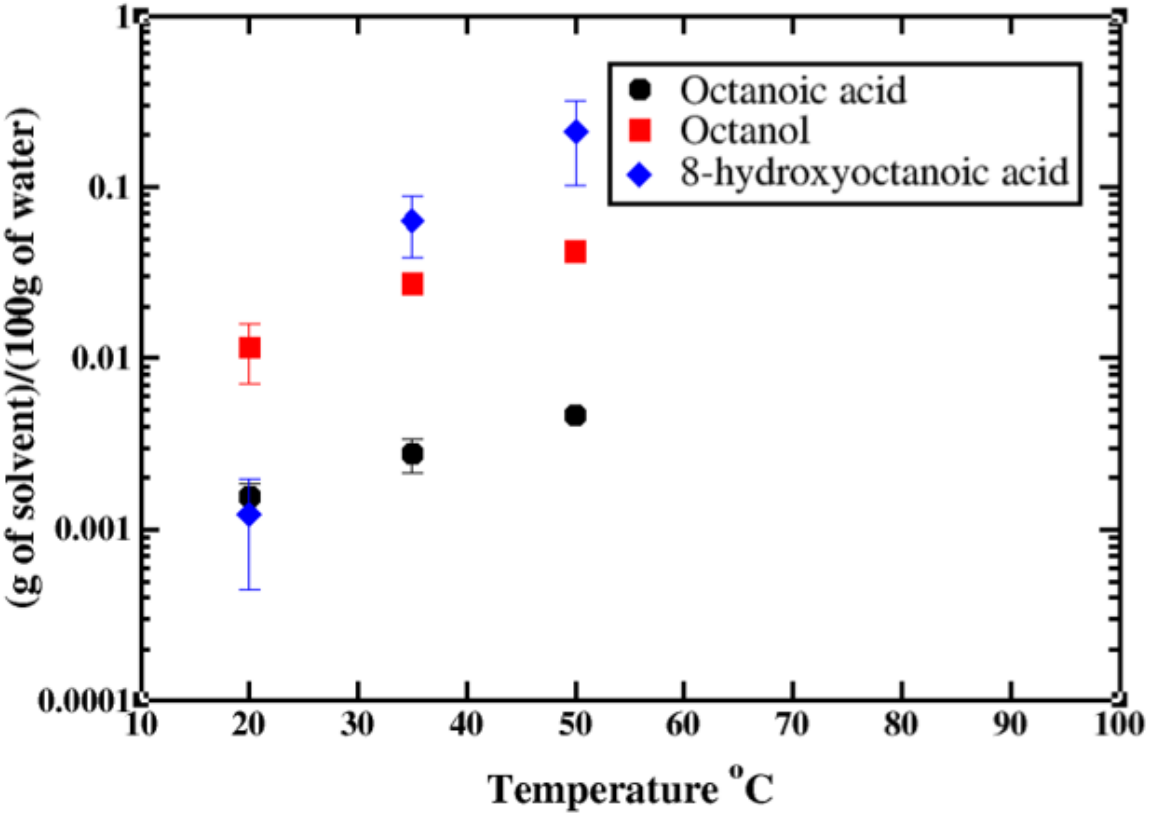

Figure 4.13: Solubility of solvent in water rich phase for branched and fluorinated structures

Having studied the properties of both octanoic acid and octanol, we were able to figure out the molecular level interactions which brings about the observable macroscopic properties. It would be interesting to see how the carboxylic acid and alcohol functional group work together. For that purpose, we started with 8-hydroxyoctanoic acid, a dual functional group molecule consisting of the -OH functional group on one end and the -COOH functional group on the other end. The structure of octanol and 8-hydroxyoctanoic acid along with octanoic acid can be seen in figure 4.11. In the case of water solubility and extraction capacity, we see that 8-hydroxyoctanoic acid performs almost as that of octanol with an effectiveness of 14.79 kg/m^3. This behavior is as expected. However, in the case of solvent loss, we see that atleast at lower temperatures 8-hydroxyoctanoic acid has got substantially lower solubility in the water phase than octanol and on par or slightly lesser than 8-hydroxyoctanoic

acid. This is again caused by the higher free energy of transfer resulting from the increase in the mass and the size of the molecule. A higher cavity would have to be made in the water box and a huge penalty is incurred for removing a molecule from the solvent phase because of the strong hydrogen bonding interactions with the surroundings.

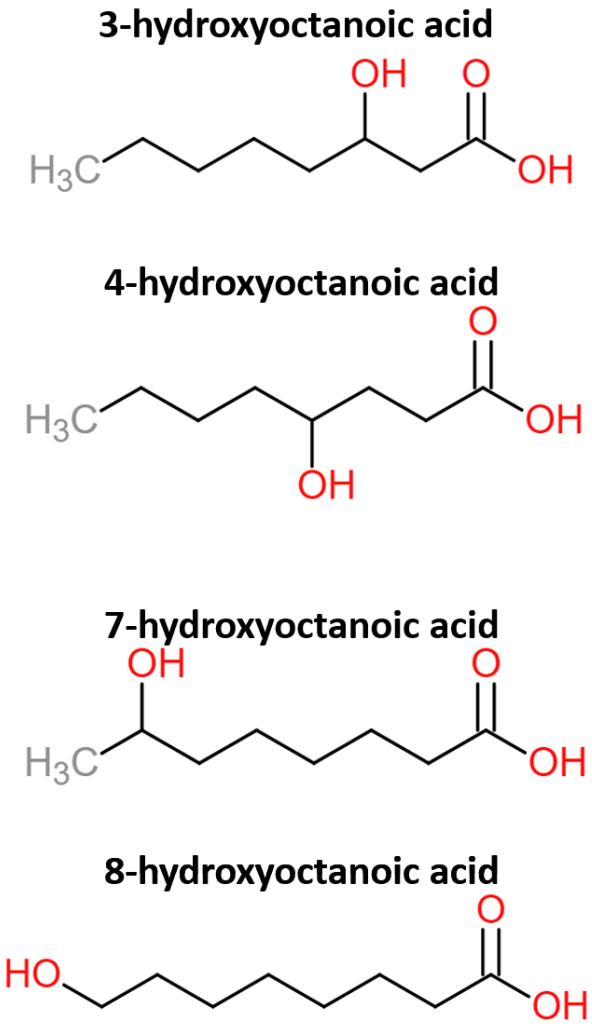

Figure 4.14: Structures used with different position of -OH group in hydroxyoctanoic acids

4.1.6 Effect of Position of the -OH Group in Hydroxyoctanoic Acids

Having got interesting results from the simulations of 8-hydroxyoctanoic acid, it was decided to see the impact of changing the position of the -OH group on the molecule. That is, different isomers of 8-hydroxyoctanoic acid. The rationale for this kind of study is that the relative position of the alcohol and the carboxylic acid group on the molecule could affect their interaction and hence the phase equilibria would be affected by this change in intramolecular interactions.

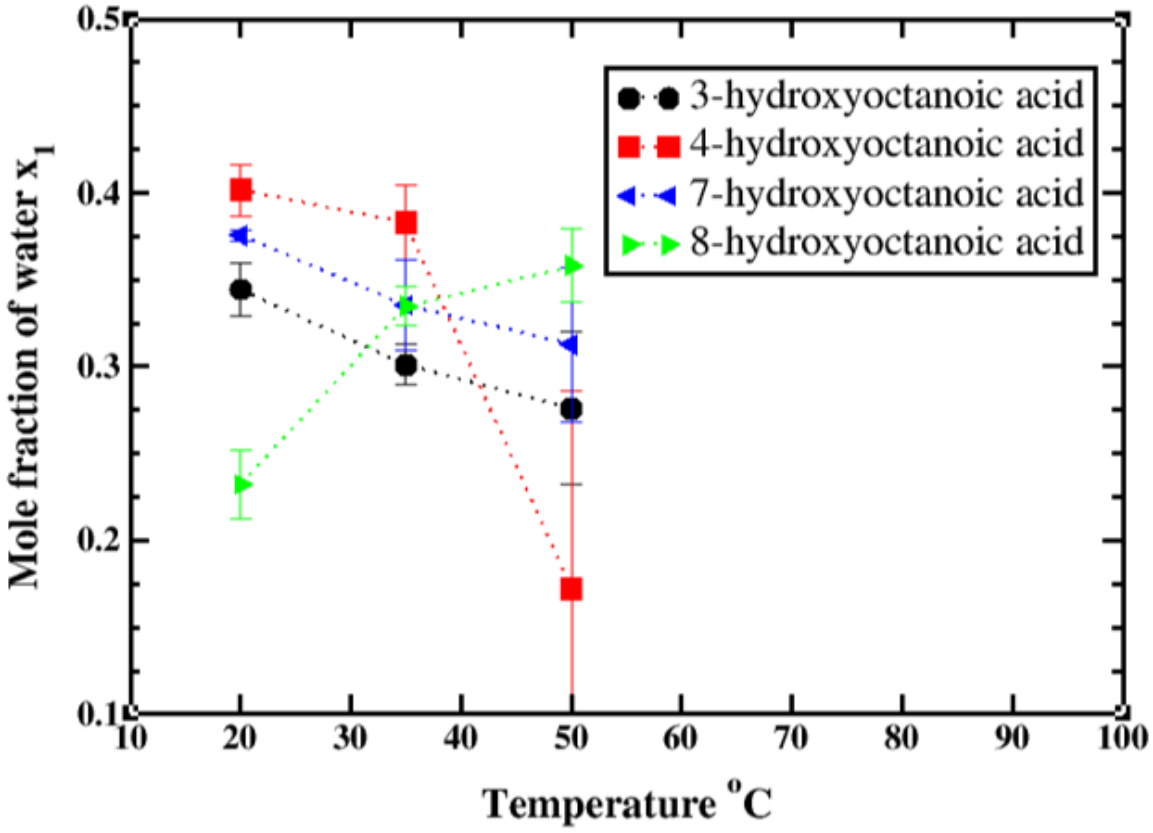

Figure 4.15: Solubility of water in solvent rich phase for isomers of hydroxyoctanoic acid

The isomers were 3-hydroxyoctanoic acid, 4-hydroxyoctanoic acid and 7-hydroxyoctanoic acid in addition to 8-hydroxyoctanoic acid which was studied as described in the previous section and their effectiveness were calculated to be -7.89 kg/m^3, -26.78 kg/m^3

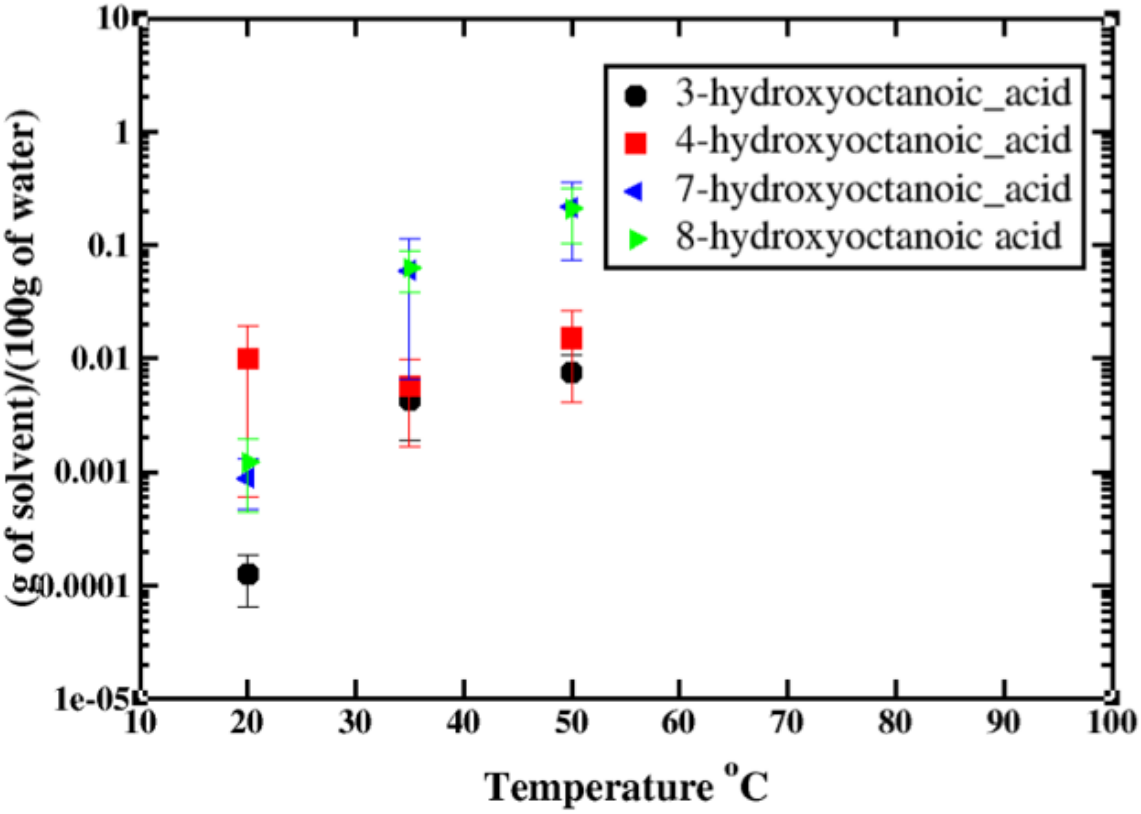

Figure 4.16: Solubility of solvent in water rich phase for isomers of hydroxyoctanoic acid

and -7.39 kg/m^3, respectively. The molecular structures of these isomers can be seen in figure 4.14. Figure 4.15 and figure 4.16 gives the equilibrium composition of the solvent rich phase and water rich phase respectively for these systems. We see that, in the case of solvent rich phase, all compounds except 8-hydroxyoctanoic acid have a reducing solubility of water with the increase in temperature which can also be inferred from the negative effectiveness. Thus it is apparent that they show a lower critical temperature as opposed to 8-hydroxyoctanoic acid and all the other solvents studied in this work, which has a upper critical solution temperature. This seems to be a puzzling behavior since these isomers are not very much chemically different to 8-hydroxyoctanoic acid but show a completely different behavior. One possible reason is that 8-hydroxyoctanoic acid is a linear structure whereas the other isomers are branched and there is a possible cross linking between the functional groups which

can form a cavity between the molecules. However, a solvent possessing a lower critical solution temperature can still be used for directional solvent extraction. These solvents has to be contacted with and phase separated from saline water at a lower temperature and then heat up the phase separated solvent to extract out the dissolved pure water. Of all these solvents, we see that 4-hydroxyoctanoic acid has got the highest effectiveness or water extraction capacity. 4-hydroxyoctanoic acid has got the -OH group right at the middle and thus possibly giving it the temperature dependence. 3-hydroxyoctanoic acid and 7-hydroxyoctanoic acid have a lower water extraction capacity as they are close to a linear structure than 4-hydroxyoctanoic acid. For the solvent loss in the water phase, we see that, 3-hyroxyoctanoic acid has got the least solubility and this is as expected since the polar functional groups for this structure is on the one end and the non-polar alkyl chain remains isolated on the other side, whereas in all the other cases, the alkyl chain is inhibited by the alcohol group thus resulting in a higher solubility. Especially, 4-hydroxyoctanoic acid has got the highest solubility at 20°C because of its highly branched structure compared to the rest of the isomers.

4.2 Mutual Solubility of Butanol-Water

As previously stated, since it would be useful to develop a molecular simulation methodology for binary LLE prediction from the already available method, we have studied the mutual solubility of Butanol-Water system using the method developed as described in chapter 2. After determining the molar volume and the residual chemical potential of both butanol and water, the logarithm of activity coefficient was determined using equation 2.15 and 2.16 and shown in figure 4.17 (symbols) for the temperature of 298.15 K. We see that the overall trend looks pretty smooth.

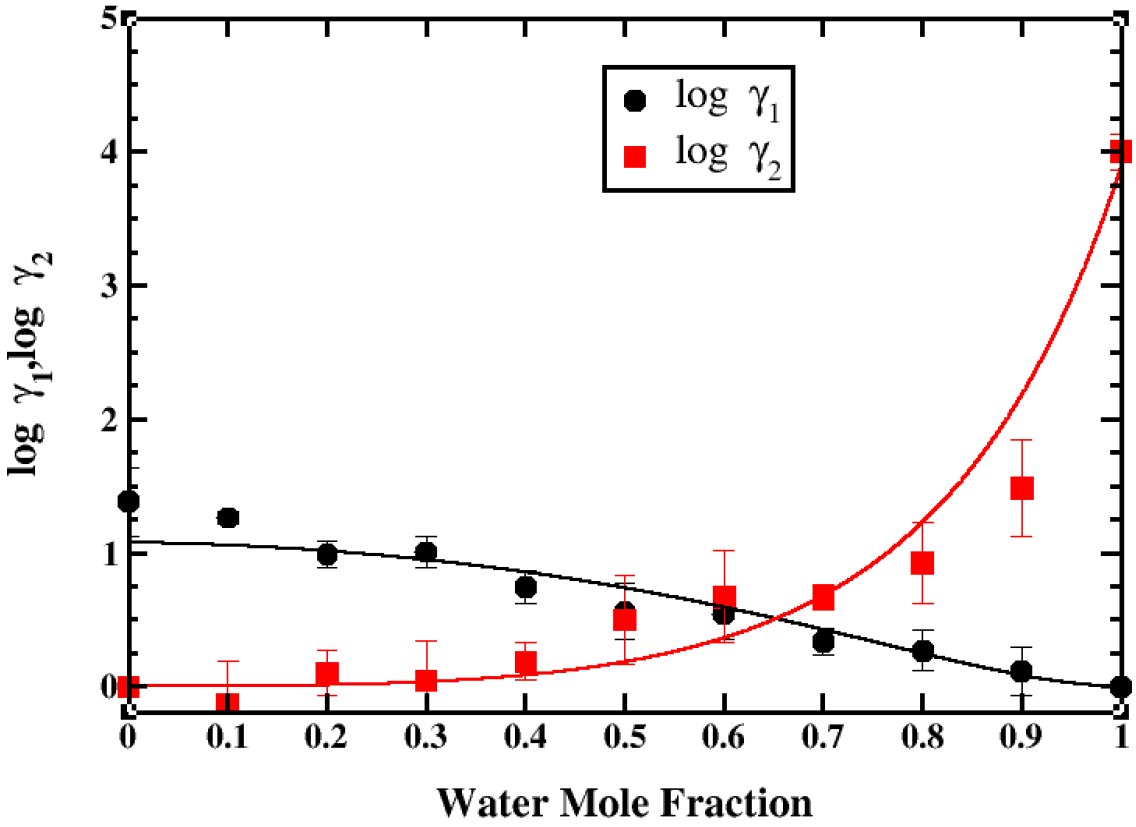

Figure 4.17: Activity coefficient plot for Butanol-Water Mixture at 298.15 K

In order to determine the equilibrium composition of the butanol rich and water rich phase, this data has to fitted to an activity coefficient model. In this work, we have used the Non-Random Two-Liquid (NRTL) model for fitting the data given by the solid curves exclusively at each temperature. The activity coefficient of the two components water(1) and butanol(2) is given as follows:

$$\log \gamma_1 = {x_2}^2 \left[\tau_{21} \left(\frac{G_{21}}{x_1 + x_2 G_{21}} \right)^2 + \frac{\tau_{12} G_{12}}{(x_2 + x_1 G_{12})^2} \right] \tag{4.2}$$

$$\log \gamma_2 = {x_1}^2 \left[\tau_{12} \left(\frac{G_{12}}{x_2 + x_1 G_{12}} \right)^2 + \frac{\tau_{21} G_{21}}{(x_1 + x_2 G_{21})^2} \right] \tag{4.3}$$

$$\log G_{12} = -\alpha_{12} \tau_{12} \tag{4.4}$$

$$\log G_{21} = -\alpha_{21} \tau_{21} \tag{4.5}$$

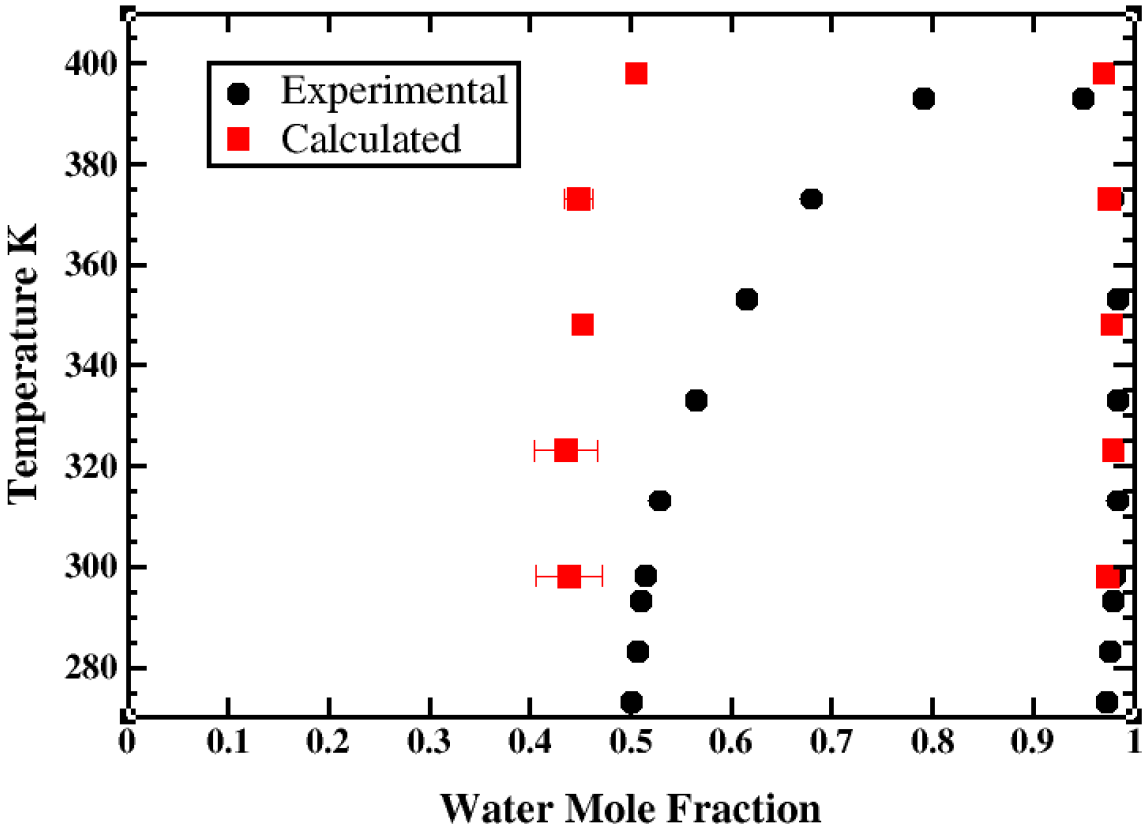

Figure 4.18: Composition of the butanol and water rich phase for the binary water(1)-butanol(2) system

The non-randomness parameters α_{12} and α_{21} was set to 0.2 following the general convention for liquid-liquid equilibria. After regression, it was found that at 298.15 K the interaction parameters τ_{12} and τ_{21} was found to be 4.503 $\pm$ 0.093 and -0.703 $\pm$ 0.118, respectively. Now that we have a model for the acitivity coefficients, equation 2.17 and 2.18 can be solved simultaneously to give the equilibrium composition x_1' and x_1'' which corresponds to the water rich phase and butanol rich phase respectively.

The solubility was calculated at five temperatures namely 298.15 K, 323.15 K, 348.15 K, 373.15 K and 398.15 K. The arising binary LLE plot is given in figure 4.18 and is compared with experimental data. We see that the calculated equilibrium compositions have reasonably good predictions with the experimental data. It can be clearly seen that the water rich phase has been very well captured. However, in the

case of butanol rich phase, we see that the calculated solubilities are slightly offset to the experimental values. This is possibly caused by the under-prediction of the butanol-water molecular level interaction by the molecular models used. This can however be artificially improved by tuning the cross interaction parameter. Thus we can tune the predictions to experimental solubility. Nonetheless, in spite of the difficulties associated with the prediction of LLE by molecular simulations, the method developed is more straightforward and is devoid of the sampling problems which can be seen in the case of Monte Carlo simulations.

CHAPTER 5

Conclusion

In this work, we have developed a molecular simulation based approach for designing, studying and screening solvents suitable for Directional Solvent Extraction (DSE) desalination. The method is based on the computation of liquid-liquid equilibria for binary systems in which one phase can be considered pure while the other contains appreciable quantities of both the components. The method relies on finding the concentration at which the fugacity of the component with appreciable solubility in both the phases is identical. In doing so, an expression relating the fugacity of a species to its mole fraction, residual chemical potential and the mixture molar volume was utilized and an expression to calculate the solubility of sparingly soluble component was derived in terms of the residual chemical potentials of the components in both the phases. The applicability of the method was demonstrated by computing the solubility of water in directional solvents namely hexanoic acid, octanoic acid, and decanoic acid as a function of temperature using the OPLS-AA force field for the acids and TIP4P model for water. The results showed that the predictions were in very good agreement with the experimental measurements. For shorter hexanoic acid, the OPLS-AA was found to yield water solubilities that were consistently lower than those reported experimentally. Lack of treating the dissociation of carboxylic acids caused under-predictions of solubilities under dilute conditions. Microscopic structural investigations showed that the solubility of water molecules in fatty acids is primarily driven by its hydrogen bonding interaction with the carboxylic acid group.

From the methodological perspective, it was observed that the statistical errors in the fugacity were predominantly associated with the corresponding errors in the residual chemical potential determination. Thus, free energy methods with low statistical uncertainty have the potential to improve the phase equilibrium predictions using the proposed method. Nonetheless, currently this method can be used for any binary systems wherein the solubility of one of the component is dilute in the other phase.

The developed method was used to study 2-propylpentanoic acid, a branched isomer of octanoic acid. It was found that it increases both the water extracting effectiveness as well as the loss in the water phase caused by the decrease in the hydrophobicity of the alkyl chain. On fluorinating the end methyl groups of 2-propylpentanoic acid, it was found that the loss in the water phase was reduced and at the same time, the water extraction capacity of 2-propylpentanoic acid was moderately preserved. This was helped by the hydrophobic nature of the fluorine groups which increased the free energy of transfer into the water phase thus reducing the solubility. All these shows that fluorinated 2-propylpentanoic acid can be a viable substitute for octanoic acid as a DSE solvent.

The addition of alcohol group to the octanoic acid structure, thus resulting in a dual functional group molecule, seems to give encouraging and positive results. 8-hydroxyoctanoic acid gave an intermediate performance between octanol and octanoic acid with a five fold increase in the effectiveness when compared with octanoic acid since it possesses the characteristic of both the functional groups. Interestingly at lower temperature, 8-hydroxyoctanoic acid has got relatively less loss of solvent in the water phase when compared to octanol and octanoic acid. This is caused by the increased size of the molecule and the strong interaction in the solvent phase creating a high free energy barrier. What this shows is that 8-hydroxyoctanoic acid would con-

taminate the produced pure water lesser than that of octanoic acid which is an already established decent DSE solvent. At the same time, we can expect 8-hydroxyoctanoic acid to have a higher loss into the saline phase since it has more solubility in water at increased temperatures. This might not be an alarming concern, provided that the solvent is not very expensive. Furthermore, when the position of the alcohol group was varied, it was found that for all the structures other that 8-hydroxyoctanoic acid, there is an inverted solubility dependence of temperature. In other words, they have got a lower critical solution temperature as opposed to all the other solvents studied which had a upper critical solution temperature. Among all the solvents studied in the work, 4-hydroxyoctanoic acid has got the highest effectiveness with more that nine times higher than octanoic acid. However, A high loss in the water phase at low temperature is observed. Further study and analysis from a molecular level perspective can unravel the reason for this unusual behavior. However, the current hypothesis is that the alcohol group is branched onto the alkyl chain unlike 8-hydroxyoctanoic acid, which has a linear structure. Thus there is a possibility of cross linking with the surrounding molecules. This increases the entropic contribution to the solubility bringing about the inverted behavior. For the loss of solvent, 3-hydroxyoctanoic acid performs the best because of the accumulation of the functional group on one end and leaving the alkyl chain intact. 4-hydroxyoctanoic acid has the highest solvent loss and this is as expected since it has a highly branched structure when compared to the other isomers. Hence, it can be concluded that, among the hydroxycarboxylic acids studied in this work, 8-hydroxyoctanoic acid has a very good improvement in effectiveness from octanoic acid and at the same time has lower loss in water phase atleast at the lower temperature.

Since most of the liquid-liquid equilibria systems are known to posses appreciable mutual solubility in both the directions, it was decided to extend the developed

method of LLE predictions suitable for any LLE problem. Binary butanol-water system was considered to demonstrate the developed method. The fugacity equation was rewritten to get the activity coefficient. Using this, the activity coefficient data was generated as a function of concentration and fitted to NRTL model from which the binary phase equilibria curve was generated. It was seen to having good agreements with experimental data and can further be improves by tuning the cross interaction between butanol and water.

CHAPTER 6

Future Directions

It was seen that flourinated 2-propylpentanoic acid has got all the good characteristics required for a DSE solvent and thus molecular simulation study of more fluorinated structures can be carried out to identify promising solvents and at the same time it is recommended that experimental studies on the fluorination of directional solvents can be carried out. This can open up a lot of opportunities to make DSE a better desalination technology for sea water desalination and the treatment of produced water resulting from the hydraulic fracturing of the oil and gas wells.

In the case of hydroxycarboxylic acids, it is recommended to further study the molecular properties of these dual functional group molecules and explore other similar structures to bring about a structure-property relationship for the properties of interest. Other functional groups such as amines, ketones and ethers can be studied and added to octanoic acid and decanoic acid structures. Using the developed method, this kind of a study has become a lot more feasible and can help in high-throughput screening of many solvents suitable for DSE and the promising solvents can be proposed for further experimental investigations.

This work does not consider the salt ion rejection abilities of the solvents. Since it is one of the important properties which affects the quality of the extracted fresh water, in the future work it is highly recommended to study and compare the free energy barrier for the solubility of salt ions from the saline water to the solvent phase.

The mutual solubility method developed in this work is free of sampling challenges that are usually seen in Gibbs Ensemble Monte Carlo (GEMC) and hence can be used for studying challenging LLE problems in the field of molecular simulations. Studying more complex and common LLE systems to well establish the developed method is proposed as a future work.

References

[1] A. Maddocks, Water stress by country (2018).
URL http://www.wri.org/resources/charts-graphs/water-stress-country

[2] The global risks report 2017 (2018).
URL https://www.weforum.org/reports/the-global-risks-report-2017/

[3] M. M. Mekonnen, A. Y. Hoekstra, Four billion people facing severe water scarcity, Science Advances 2 (2). doi:10.1126/sciadv.1500323.
URL http://advances.sciencemag.org/content/advances/2/2/e1500323.full.pdf

[4] H. Perlman, The world's water (2018).
URL https://water.usgs.gov/edu/earthwherewater.html

[5] M. Elimelech, W. A. Phillip, The future of seawater desalination: Energy, technology, and the environment, Science 333 (6043) (2011) 712–717. doi:10.1126/science.1200488.
URL http://science.sciencemag.org/content/sci/333/6043/712.full.pdf

[6] M. A. Shannon, P. W. Bohn, M. Elimelech, J. G. Georgiadis, B. J. Marinas, A. M. Mayes, Science and technology for water purification in the coming decades, Nature 452 (7185) (2008) 301–10. doi:10.1038/nature06599.

[7] N. Voutchkov, Desalination âĂŞ past, present and future (2018).
URL http://www.iwa-network.org/desalination-past-present-future/

[8] N. Ghaffour, T. M. Missimer, G. L. Amy, Technical review and evaluation of the economics of water desalination: Current and future challenges for better water supply sustainability, Desalination 309 (2013) 197–207. doi:https://doi.org/10.1016/j.desal.2012.10.015.
URL http://www.sciencedirect.com/science/article/pii/S0011916412005723

[9] A. Bajpayee, T. Luo, A. Muto, G. Chen, Very low temperature membrane-free desalination by directional solvent extraction, Energy & Environmental Science 4 (5) (2011) 1672–1675. doi:10.1039/C1EE01027A.
URL http://dx.doi.org/10.1039/C1EE01027A

[10] T. Luo, A. Bajpayee, G. Chen, Directional solvent for membrane-free water desalinationâĂŤA molecular level study, Journal of Applied Physics 110 (5) (2011) 054905. doi:10.1063/1.3627239.
URL http://aip.scitation.org/doi/abs/10.1063/1.3627239

[11] D. Rish, S. Luo, B. Kurtz, T. Luo, Exceptional ion rejection ability of directional solvent for non-membrane desalination, Applied Physics Letters 104 (2) (2014) 024102. doi:10.1063/1.4861835.
URL http://aip.scitation.org/doi/abs/10.1063/1.4861835

[12] D. B. Sanap, K. D. Kadam, M. Narayan, S. Kasthurirangan, P. R. Nemade, V. H. Dalvi, Analysis of saline water desalination by directed solvent extraction using octanoic acid, Desalination 357 (2015) 150–162. doi:https://doi.org/10.1016/j.desal.2014.11.020.
URL http://www.sciencedirect.com/science/article/pii/S0011916414006110

[13] S. Alotaibi, O. M. Ibrahim, S. Luo, T. Luo, Modeling of a continuous water desalination process using directional solvent extraction, Desalination 420 (2017)

114–124. doi:https://doi.org/10.1016/j.desal.2017.07.004.
URL http://www.sciencedirect.com/science/article/pii/S0011916417304277

[14] A. Z. Panagiotopoulos, Direct determination of phase coexistence properties of fluids by Monte Carlo simulation in a new ensemble, Molecular Physics 61 (4) (1987) 813–826. doi:10.1080/00268978700101491.
URL https://doi.org/10.1080/00268978700101491

[15] A. Z. Panagiotopoulos, N. Quirke, M. Stapleton, D. J. Tildesley, Phase equilibria by simulation in the Gibbs ensemble, Molecular Physics 63 (4) (1988) 527–545. doi:10.1080/00268978800100361.
URL https://doi.org/10.1080/00268978800100361

[16] M. E. van Leeuwen, C. J. Peters, J. de Swaan Arons, A. Z. Panagiotopoulos, Investigation of the transition to liquid-liquid immiscibilitym for Lennard-Jones (12,6) systems, using Gibbs-ensemble molecular simulations, Fluid Phase Equilibria 66 (1) (1991) 57–75. doi:https://doi.org/10.1016/0378-3812(91)85047-X.
URL http://www.sciencedirect.com/science/article/pii/037838129185047X

[17] S. M. Lambert, D. S. Soane, J. M. Prausnitz, Liquid-Liquid Equilibria in Binary Systems:Monte-Carlo Simulations for Calculating the Effect of Nonrandom Mixing, Fluid Phase Equilibria 83 (1993) 59–68. doi:https://doi.org/10.1016/0378-3812(93)87007-N.
URL http://www.sciencedirect.com/science/article/pii/037838129387007N

[18] M. H. Lamm, C. K. Hall, Monte Carlo simulations of complete phase diagrams for binary LennardâĂŞJones mixtures, Fluid Phase Equilibria 182 (1) (2001)

37–46. doi:https://doi.org/10.1016/S0378-3812(01)00378-8.
URL http://www.sciencedirect.com/science/article/pii/S0378381201003788

[19] D. G. Green, G. Jackson, E. d. Miguel, L. F. Rull, VaporâĂŞliquid and liquidâĂŞliquid phase equilibria of mixtures containing squareâĂŘwell molecules by Gibbs ensemble Monte Carlo simulation, The Journal of Chemical Physics 101 (4) (1994) 3190–3204. doi:10.1063/1.467565.
URL http://aip.scitation.org/doi/abs/10.1063/1.467565

[20] R. J. Sadus, RESEARCH NOTE Molecular simulation of the liquid-liquid equilibria of binary mixtures containing dipolar and non-polar components interacting via the Keesom potential, Molecular Physics 89 (4) (1996) 1187–1194. doi:10.1080/002689796173589.
URL https://doi.org/10.1080/002689796173589

[21] B. Chen, J. I. Siepmann, Partitioning of Alkane and Alcohol Solutes between Water and (Dry or Wet) 1-Octanol, Journal of the American Chemical Society 122 (27) (2000) 6464–6467. doi:10.1021/ja001120+.
URL http://dx.doi.org/10.1021/ja001120+

[22] I. Brovchenko, B. Guillot, Simulation of the liquidâĂŞliquid coexistence of the tetrahydrofuran+water mixture in the Gibbs ensemble, Fluid Phase Equilibria 183-184 (2001) 311–319. doi:https://doi.org/10.1016/S0378-3812(01)00443-5.
URL http://www.sciencedirect.com/science/article/pii/S0378381201004435

[23] L. Zhang, J. I. Siepmann, Pressure Dependence of the VaporâĹŠLiquidâĹŠLiquid Phase Behavior in Ternary Mixtures Consisting of n-Alkanes, n-Perfluoroalkanes,

and Carbon Dioxide, The Journal of Physical Chemistry B 109 (7) (2005) 2911–2919. doi:10.1021/jp0482114.
URL http://dx.doi.org/10.1021/jp0482114

[24] S. Moodley, E. Johansson, K. Bolton, D. Ramjugernath, Gibbs ensemble Monte Carlo simulations of binary vapourâĂŞliquidâĂŞliquid equilibrium: application to n-hexaneâĂŞwater and ethaneâĂŞethanol systems, Molecular Simulation 36 (10) (2010) 758–762. doi:10.1080/08927021003752820.
URL https://doi.org/10.1080/08927021003752820

[25] S. Moodley, K. Bolton, D. Ramjugernath, Monte Carlo simulations of vaporâĂŞliquidâĂŞliquid equilibrium of some ternary petrochemical mixtures, Fluid Phase Equilibria 299 (1) (2010) 24–31. doi:https://doi.org/10.1016/j.fluid.2010.08.015.
URL http://www.sciencedirect.com/science/article/pii/S0378381210004188

[26] P. Bai, J. I. Siepmann, Gibbs ensemble Monte Carlo simulations for the liquidâĂŞliquid phase equilibria of dipropylene glycol dimethyl ether and water: A preliminary report, Fluid Phase Equilibria 310 (1) (2011) 11–18. doi:https://doi.org/10.1016/j.fluid.2011.06.003.
URL http://www.sciencedirect.com/science/article/pii/S0378381211002627

[27] M. Lasich, E. L. Johansson, D. Ramjugernath, Assessing the ability of force-fields to predict liquidâĂŞliquid equilibria of ternary systems of light alcohols+water+dodecane by Monte Carlo simulation, Fluid Phase Equilibria 368 (2014) 65–71. doi:https://doi.org/10.1016/j.fluid.2014.02.002.
URL http://www.sciencedirect.com/science/article/pii/S0378381214000855

[28] D. B. Harwood, C. J. Peters, J. I. Siepmann, A Monte Carlo simulation study of the liquidâĂŞliquid equilibria for binary dodecane/ethanol and ternary dodecane/ethanol/water mixtures, Fluid Phase Equilibria 407 (2016) 269–279. doi:https://doi.org/10.1016/j.fluid.2015.07.011.
URL http://www.sciencedirect.com/science/article/pii/S0378381215300261

[29] J. I. Siepmann, D. Frenkel, Configurational bias Monte Carlo: a new sampling scheme for flexible chains, Molecular Physics 75 (1) (1992) 59–70. doi:10.1080/00268979200100061.
URL https://doi.org/10.1080/00268979200100061

[30] J. J. de Pablo, M. Laso, J. I. Siepmann, U. W. Suter, Continuum-configurational-bias Monte Carlo simulations of long-chain alkanes, Molecular Physics 80 (1) (1993) 55–63. doi:10.1080/00268979300102061.
URL https://doi.org/10.1080/00268979300102061

[31] M. G. Martin, J. I. Siepmann, Novel Configurational-Bias Monte Carlo Method for Branched Molecules. Transferable Potentials for Phase Equilibria. 2. United-Atom Description of Branched Alkanes, The Journal of Physical Chemistry B 103 (21) (1999) 4508–4517. doi:10.1021/jp984742e.
URL http://dx.doi.org/10.1021/jp984742e

[32] C. D. Wick, J. I. Siepmann, Self-Adapting Fixed-End-Point Configurational-Bias Monte Carlo Method for the Regrowth of Interior Segments of Chain Molecules with Strong Intramolecular Interactions, Macromolecules 33 (19) (2000) 7207–7218. doi:10.1021/ma000172g.
URL http://dx.doi.org/10.1021/ma000172g

[33] J. K. Shah, E. J. Maginn, A general and efficient monte carlo method for sampling intramolecular degrees of freedom of branched and cyclic molecules, The Journal of Chemical Physics 135 (13) (2011) 134121. doi:10.1063/1.3644939.

[34] W. Shi, E. J. Maginn, Continuous Fractional Component Monte Carlo:âĂŁ An Adaptive Biasing Method for Open System Atomistic Simulations, Journal of Chemical Theory and Computation 3 (4) (2007) 1451–1463. doi:10.1021/ct7000039.
URL http://dx.doi.org/10.1021/ct7000039

[35] W. Shi, E. J. Maginn, Improvement in molecule exchange efficiency in Gibbs ensemble Monte Carlo: Development and implementation of the continuous fractional component move, Journal of Computational Chemistry 29 (15) (2008) 2520–2530. doi:10.1002/jcc.20977.
URL http://dx.doi.org/10.1002/jcc.20977

[36] J. N. C. Lopes, D. J. Tildesley, Multiphase equilibria using the Gibbs ensemble Monte Carlo method, Molecular Physics 92 (2) (1997) 187–196. doi:10.1080/002689797170392.
URL http://www.tandfonline.com/doi/abs/10.1080/002689797170392

[37] T. I. Morrow, E. J. Maginn, Isomolar semigrand ensemble molecular dynamics: Development and application to liquid-liquid equilibria, The Journal of Chemical Physics 122 (5) (2005) 054504. doi:10.1063/1.1839172.
URL http://aip.scitation.org/doi/abs/10.1063/1.1839172

[38] T. Cheng, F. Li, J. Dai, H. Sun, Prediction of the mutual solubility of water and dipropylene glycol dimethyl ether using molecular dynamics simulation, Fluid Phase Equilibria 314 (2012) 1–6. doi:https://doi.org/10.1016/j.fluid.2011.10.013.

URL http://www.sciencedirect.com/science/article/pii/S0378381211004924

[39] L. D. Gelb, E. A. MÃijller, Location of phase equilibria by temperature-quench molecular dynamics simulations, Fluid Phase Equilibria 203 (1) (2002) 1–14. doi:https://doi.org/10.1016/S0378-3812(02)00174-7.
URL http://www.sciencedirect.com/science/article/pii/S0378381202001747

[40] S. Eckelsbach, T. Windmann, E. Elts, J. Vrabec, Simulation of Liquid-Liquid Equilibria with Molecular Models Optimized to Vapor-Liquid Equilibria and Model Development for Hydrazine and Two of Its Derivatives, High Performance Computing in Science and Engineering âĂŸ12, Springer Berlin Heidelberg, 2013, pp. 451–460.

[41] A. S. Paluch, E. J. Maginn, Efficient Estimation of the Equilibrium Solution-Phase Fugacity of Soluble Nonelectrolyte Solids in Binary Solvents by Molecular Simulation, Industrial & Engineering Chemistry Research 52 (38) (2013) 13743–13760. doi:10.1021/ie401295j.
URL http://dx.doi.org/10.1021/ie401295jhttp://pubs.acs.org/doi/10.1021/ie401295j

[42] J. Noroozi, A. S. Paluch, Microscopic Structure and Solubility Predictions of Multifunctional Solids in Supercritical Carbon Dioxide: A Molecular Simulation Study, The Journal of Physical Chemistry B 121 (7) (2017) 1660–1674. doi:10.1021/acs.jpcb.6b12390.
URL http://dx.doi.org/10.1021/acs.jpcb.6b12390http://pubs.acs.org/doi/10.1021/acs.jpcb.6b12390

[43] J. G. Kirkwood, Statistical mechanics of fluid mixtures, The Journal of Chemical Physics 3 (5) (1935) 300–313. doi:10.1063/1.1749657.

[44] W. L. Jorgensen, D. S. Maxwell, J. Tirado-Rives, Development and Testing of the OPLS All-Atom Force Field on Conformational Energetics and Properties of Organic Liquids, Journal of the American Chemical Society 118 (45) (1996) 11225–11236. doi:10.1021/ja9621760.
URL http://dx.doi.org/10.1021/ja9621760http://pubs.acs.org/doi/abs/10.1021/ja9621760

[45] W. L. Jorgensen, J. Chandrasekhar, J. D. Madura, R. W. Impey, M. L. Klein, Comparison of simple potential functions for simulating liquid water, The Journal of Chemical Physics 79 (2) (1983) 926–935. doi:10.1063/1.445869.
URL http://aip.scitation.org/doi/abs/10.1063/1.445869

[46] B. Hess, P-LINCS:âĂĽ A Parallel Linear Constraint Solver for Molecular Simulation, Journal of Chemical Theory and Computation 4 (1) (2008) 116–122. doi:10.1021/ct700200b.
URL http://dx.doi.org/10.1021/ct700200bhttp://pubs.acs.org/doi/abs/10.1021/ct700200b

[47] M. J. Abraham, T. Murtola, R. Schulz, S. PÃąll, J. C. Smith, B. Hess, E. Lindahl, GROMACS: High performance molecular simulations through multi-level parallelism from laptops to supercomputers, SoftwareX 1-2 (2015) 19–25. doi:https://doi.org/10.1016/j.softx.2015.06.001.
URL http://www.sciencedirect.com/science/article/pii/S2352711015000059

[48] L. MartÃŋnez, R. Andrade, E. G. Birgin, J. M. MartÃŋnez, Packmol: A package for building initial configurations for molecular dynamics simulations, Journal of Computational Chemistry 30 (13) (2009) 2157–2164. doi:10.1002/jcc.21224.
URL http://dx.doi.org/10.1002/jcc.21224http://onlinelibrary.

wiley.com/store/10.1002/jcc.21224/asset/21224_ftp.pdf?v=1&t=jcs5z085&s=ec9a0858cbe9c5f2436e1df65ccd3b63587ac142

[49] T. Darden, D. York, L. Pedersen, Particle mesh Ewald: An NâŃĚlog(N) method for Ewald sums in large systems, The Journal of Chemical Physics 98 (12) (1993) 10089–10092. doi:10.1063/1.464397.
URL http://aip.scitation.org/doi/abs/10.1063/1.464397

[50] M. B. Oliveira, M. J. Pratas, I. M. Marrucho, A. J. Queimada, J. A. P. Coutinho, Description of the mutual solubilities of fatty acids and water with the CPA EoS, AIChE Journal 55 (6) (2009) 1604–1613. doi:10.1002/aic.11766.
URL http://dx.doi.org/10.1002/aic.11766

[51] A. W. Ralston, C. W. Hoerr, THE SOLUBILITIES OF THE NORMAL SATURATED FATTY ACIDS, The Journal of Organic Chemistry 07 (6) (1942) 546–555. doi:10.1021/jo01200a013.
URL http://dx.doi.org/10.1021/jo01200a013

[52] M. D. Barratt, Quantitative structure-activity relationships (QSARs) for skin corrosivity of organic acids, bases and phenols: Principal components and neural network analysis of extended datasets, Toxicology in Vitro 10 (1) (1996) 85–94. doi:https://doi.org/10.1016/0887-2333(95)00101-8.
URL http://www.sciencedirect.com/science/article/pii/0887233395001018

APPENDIX A

Hexanoic Acid and Decanoic Acid Supplementary Information

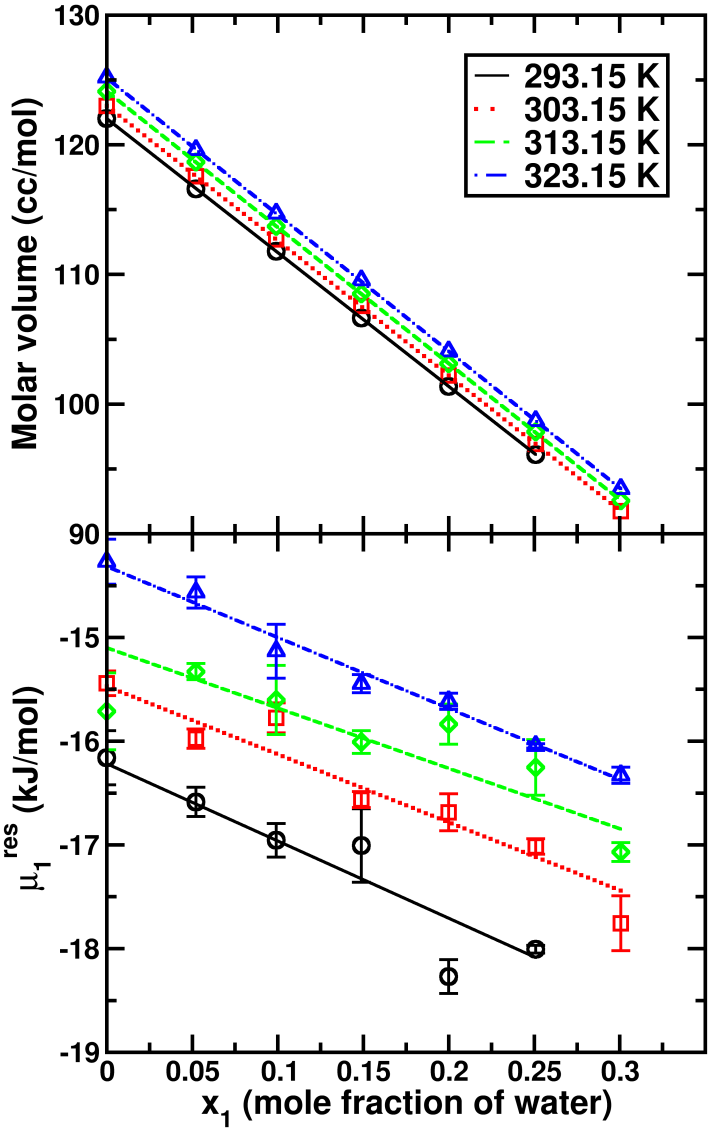

Figure A.1: Molar volume and residual chemical potential of water as a function of composition for hexanoic acid-water mixture

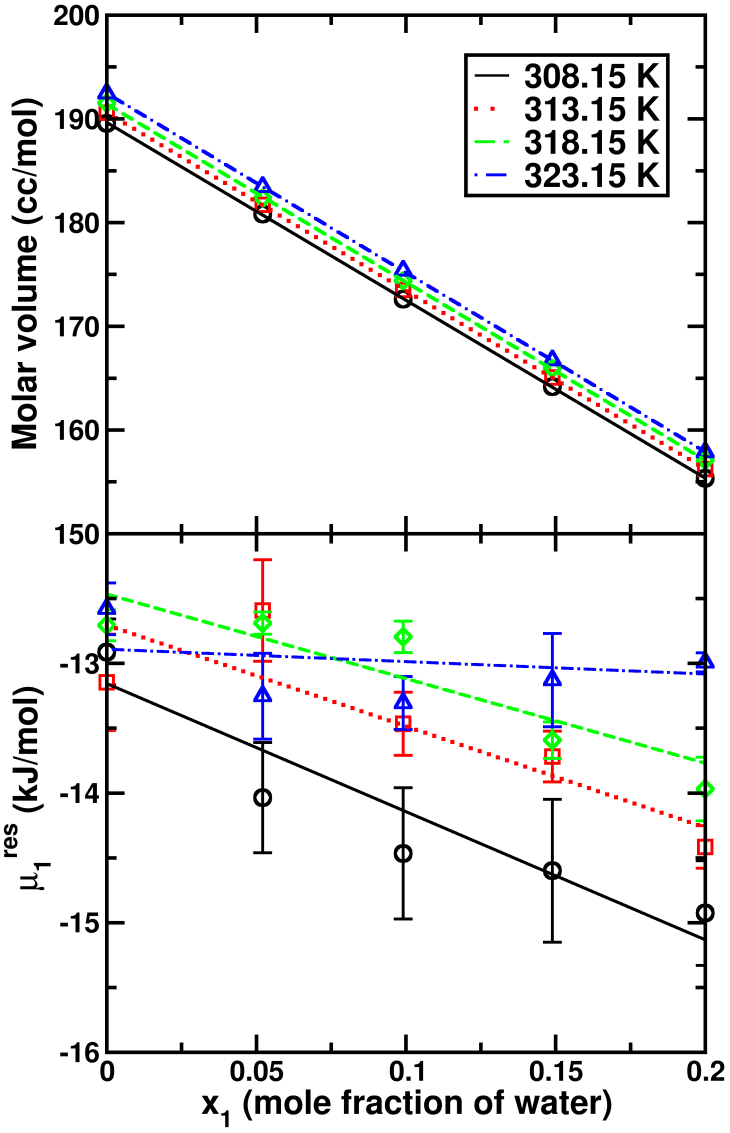

Figure A.2: Molar volume and residual chemical potential of water as a function of composition for decanoic acid-water mixture

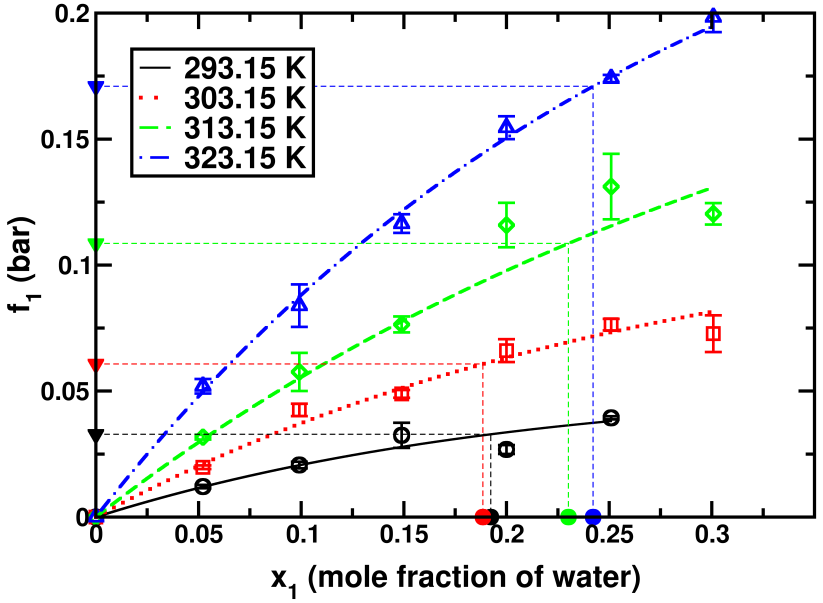

Figure A.3: Fugacity of water vs. composition plot for hexanoic acid-water mixture

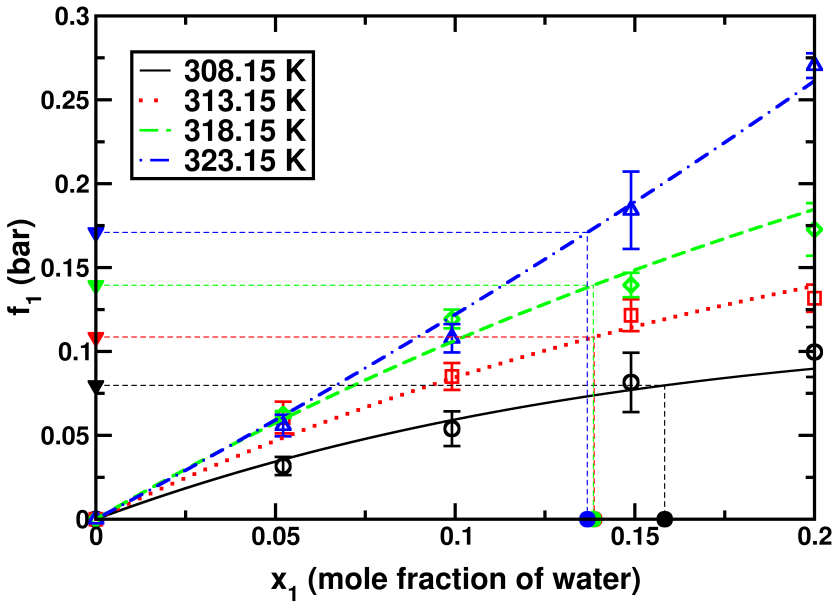

Figure A.4: Fugacity of water vs. composition plot for decanoic acid-water mixture

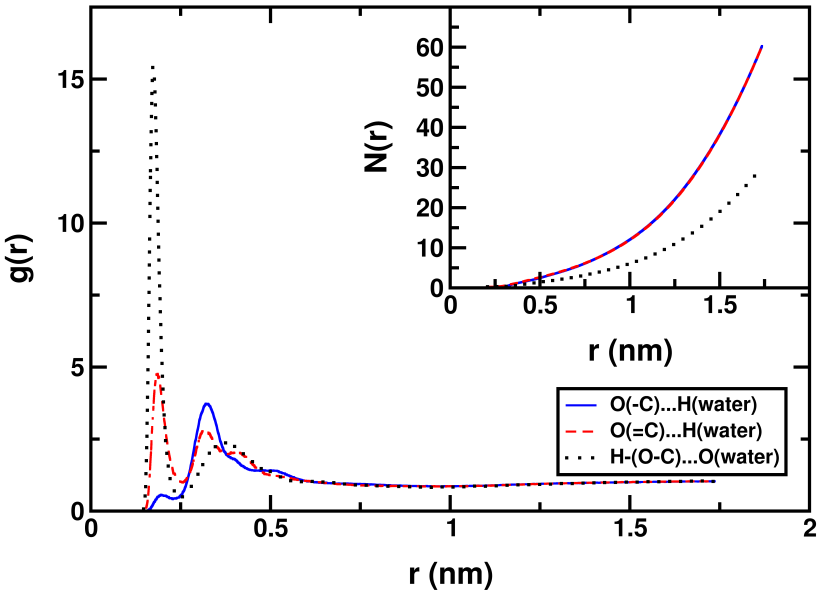

Figure A.5: Radial distribution function for hexanoic acid rich phase at 313.15 K

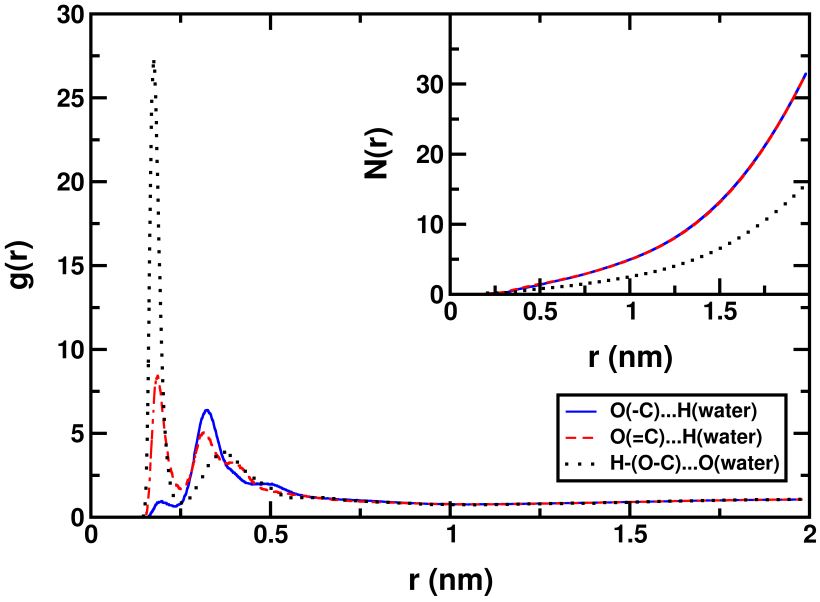

Figure A.6: Radial distribution function for decanoic acid rich phase at 313.15 K

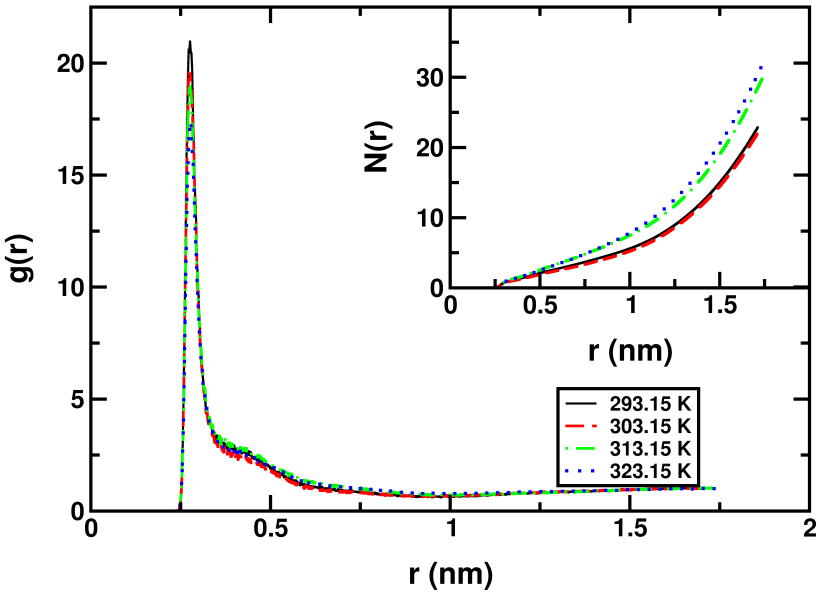

Figure A.7: Oxygen-oxygen radial distribution function for water in hexanoic acid rich phase

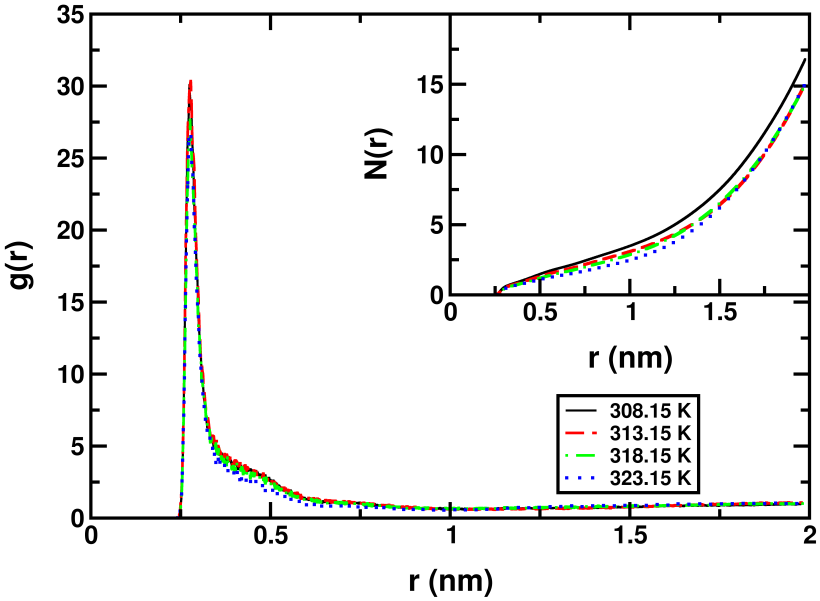

Figure A.8: Oxygen-oxygen radial distribution function for water in decanoic acid rich phase

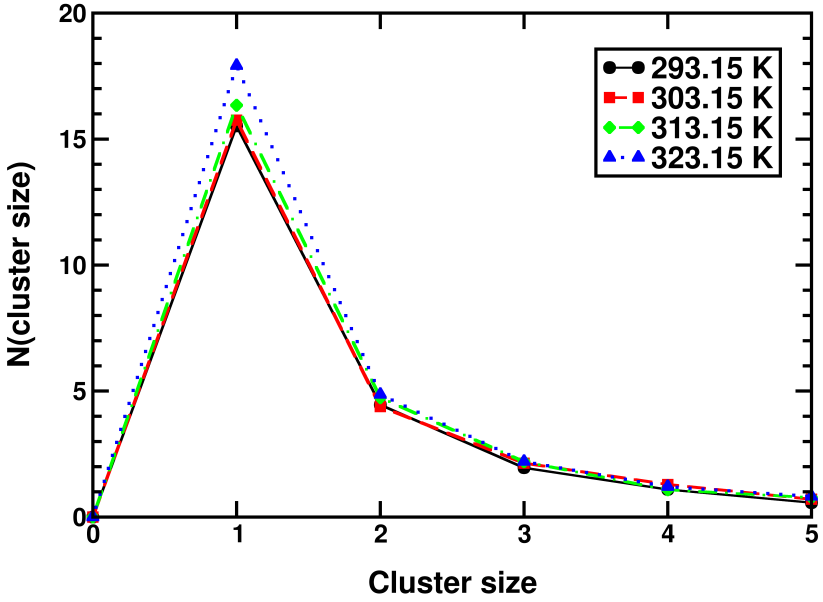

Figure A.9: Oxygen-oxygen radial distribution function for water in hexanoic acid rich phase

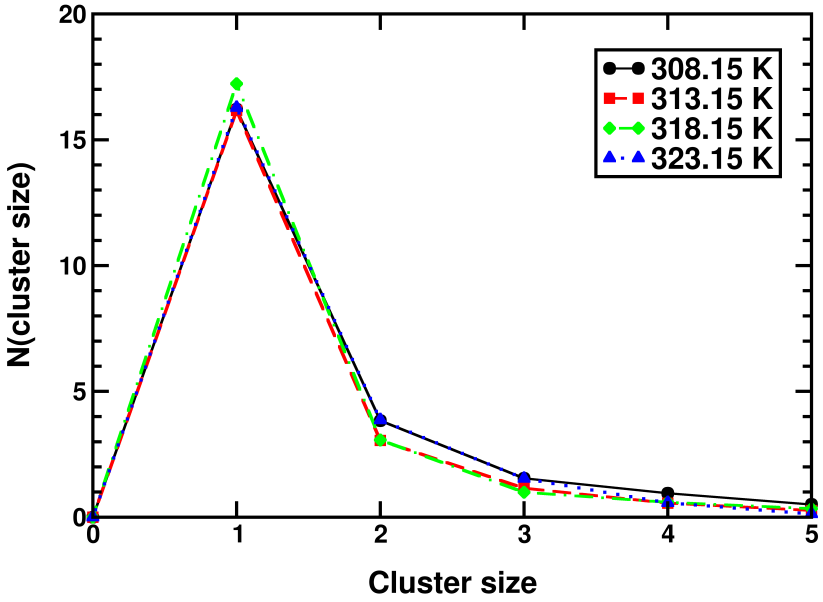

Figure A.10: Oxygen-oxygen radial distribution function for water in decanoic acid rich phase

VITA

PRASHANTH CHANDRAN

Candidate for the Degree of

Master of Science

Thesis: A NOVEL MOLECULAR SIMULATION APPROACH TO LIQUID-LIQUID EQUILIBRIA AND APPLICATION TO THE DESIGN OF DESALINATION SOLVENTS

Major Field: Chemical Engineering

Biographical:

Education:

Completed the requirements for the degree of Master of Science with a major in Chemical Engineering at Oklahoma State University in May 2108.

Received a Bachelor of Technology in Chemical Engineering at Anna University, Chennai, India in April 2016.

Experience:

Graduate Research Assistant, School of Chemical Engineering, Oklahoma State University (August 2016 - May 2018)

Research Intern, Central Leather Research Institute, Chennai, India (May 2015 - March 2016)